Mutations in Spliceosomal Gene *SNW1* Cause Neurodevelopment Disorders with Microcephaly

Lei Ji[1,2†], Jin Yan[3†], Nicole A. Losurdo[4†], Hua Wang[5,6], Liangjie Liu[1,2], Keyi Li[1,2], Zhen Liu[7,8], Zhenming Guo[3], Jing Xu[3], Adriana Bibo[4], Decheng Ren[1,2], Ke Yang[1,2], Yingying Luo[1,2], Fengping Yang[1,2], Gui Wang[3], Zhenglong Xiang[3], Yuan Wang[3], Huaizhe Zhan[3], Hu Pan[7,8], Juanli Hu[7,8], Jianmin Zhong[9], Rami Abou Jamra[10], Pia Zacher[11], Luciana Musante[12], Flavio Faletra[13,14], Paola Costa[12], Caterina Zanus[12], Nathalie Couque[15,16], Lyse Ruaud[15,16], Anna Maria Cueto-González[17,18], Hector San Nicolas Fernández[17,18], Eduardo Tizzano[17,18], Nuria Martinez Gil[17,18], Xiaorong Liu[19], Weiping Liao[19], Layal Abi Farraj[20], Alden Y. Huang[20,21], Liying Zhang[20], Aparna Murali[21], Esther Schmuel[22], Christina S. Han[21], Kayla King[23,24], Weiyue Gu[25], Pengchao Wang[25], Kai Li[26], Nichole Link[4], Guang He[1,2,8]*, Shan Bian[3,8,27]*, Xiao Mao[7,8]*

[†]**These authors contributed equally to this work.**

Author affiliations:

1. Bio-X Institutes, Key Laboratory for the Genetics of Developmental and Neuropsychiatric Disorders, Shanghai Jiao Tong University, Shanghai, China.
2. Shanghai Institute of Medical Genetics, Shanghai Children's Hospital, Shanghai Jiao Tong University School of Medicine, Shanghai, China
3. Institute for Regenerative Medicine, State Key Laboratory of Cardiology and Medical Innovation Center, Shanghai East Hospital, Frontier Science Center for Stem Cell Research School of Life Sciences and Technology, Tongji University, Shanghai, China.
4. Department of Neurobiology, University of Utah, Salt Lake, UT, USA
5. The Affiliated Children's Hospital of Xiangya School of Medicine, Central South University, Changsha, China.
6. Clinical Medical Research Center for Hereditary Birth Defects and Rare Diseases in

Hunan Province, Changsha, China.
7. Department of Medical Genetics, Hunan Provincial Maternal and Child Health Care Hospital, Changsha, China
8. National Health Commission Key Laboratory for Birth Defect Research and Prevention, Hunan Provincial Maternal and Child Health Care Hospital, Changsha, China
9. Department of Neurology, Jiangxi Provincial Children's Hospital, Nanchang, China
10. Institute of Human Genetics, University of Leipzig Medical Center, Leipzig, Germany.
11. Kleinwachau Epilepsy Center, Radeberg, Germany
12. Institute for Maternal and Child Health, IRCCS “Burlo Garofolo”, Trieste, Italy
13. Institute of Medical Genetics, Azienda Sanitaria Universitaria Friuli Centrale (ASUFC), Udine, Italy
14. Department of Medicine (DMED), University of Udine, Udine, ltaly.
15. Department of Genetics, APHP-Robert Debré University Hospital, Paris, France
16. Laboratoire de Biologie Médicale Multi-Site SeqOIA, Sorbonne University, Paris, France.
17. Department of Clinical and Molecular Genetics, Vall d'Hebron Barcelona Hospital Campus, Barcelona, Spain
18. Medicine Genetics Group, Vall Hebron Research Institute, Vall d'Hebron Barcelona Hospital Campus, Autonomous University of Barcelona, Barcelona, Spain
19. Department of Neurology, Institute of Neuroscience, Key Laboratory of Neurogenetics and Channelopathies of Guangdong Province and the Ministry of Education of China, The Second Affiliated Hospital, Guangzhou Medical University, Guangzhou, China
20. Department of Pathology and Laboratory Medicine, David Geffen School of Medicine at UCLA, Los Angeles, CA, USA
21. Department of Obstetrics and Gynecology, David Geffen School of Medicine at UCLA, Los Angeles, CA, USA
22. Comprehensive Materna Fetal Medicine Center, Thousand Oaks, CA, USA

23. Department of Human and Molecular Genetics, VCU Health School of Medicine, Richmond, VA, USA
24. Department of Pediatrics Genetics, VCU Health CHOR, Richmond, VA, USA
25. Chigene (Beijing) Translational Medical Research Center Co. Ltd, Beijing, China
26. Department of Neurology and Suzhou Clinical Research Center of Neurological Disease, The Second Affiliated Hospital of Soochow University, Suzhou, China
27. China Regional Research Centre, International Centre for Genetic Engineering and Biotechnology, Taizhou, China

* Corresponding author at: National Health Commission Key Laboratory for Birth Defect Research and Prevention, Hunan Provincial Maternal and Child Health Care Hospital, Changsha 410100, China. E-mail: gbtechies@outlook.com; Bio-X Institutes, Shanghai Jiao Tong University, 1954 Huashan Road, Shanghai 200030, China. Email: heguang@sjtu.edu.cn; School of Life Sciences and Technology, Tongji University, 1239 Siping Road, Shanghai 200092, China. E-mail: shan_bian@tongji.edu.cn.

Abstract

The spliceosome is a critical cellular machinery responsible for pre-mRNA splicing, essential for the proper expression of genes. Mutations in its core components are increasingly linked to neurodevelopmental disorders, such as primary microcephaly. Here, we investigated the role of SNW1, a spliceosomal protein, in splicing integrity and neurodevelopment. We identified nine heterozygous mutations in the *SNW1* gene in patients presenting with primary microcephaly. These mutations impaired SNW1's interactions with core spliceosomal proteins, leading to defective RNA splicing and reduced protein functionality. Using *Drosophila melanogaster* and human embryonic stem cell-derived cerebral organoids models, we demonstrated that *SNW1* depletion resulted in significant reductions in neural stem cell proliferation and increased apoptosis. RNA-sequencing revealed disrupted alternative splicing, especially skipping exons, and altered expression of neurodevelopment-associated genes (*CENPE*, *MEF2C*, and *NRXN2*). Our findings provide crucial insights into the molecular mechanisms by which *SNW1* dysfunction contributes to neurodevelopmental disorders and underscore the importance of proper spliceosome function in brain development.

Introduction

Mutations in spliceosome components—a key cellular machinery for pre-mRNA splicing—are increasingly implicated in neurodevelopmental disorders (NDDs), notably primary microcephaly (1, 2). The spliceosome, composed of five snRNAs and ~100 proteins, removes introns and joins exons to generate mature mRNA (3, 4). Beyond snRNAs, non-snRNP factors including the NineTeen complex (NTC) and NTC-related (NTR) proteins are essential for spliceosome activation and catalysis (5-8). Recent electron microscopy studies have resolved its structure at near-atomic resolution, shedding light on splicing dynamics (9). Pathogenic mutations have been identified in core spliceosomal proteins, including the exon junction complex (EJC) (10), *EFTUD2* (11, 12), *WBP4* (13), *U2AF2*, *PRP19* (2), *PPIL1* and *PRP17* (14-16). These mutations disrupt alternative splicing, which is especially conserved and functionally critical in the brain (17, 18). The high energy demand of the brain further exacerbates the impact of spliceosomal dysfunction during development (2, 19).

SNW domain-containing protein 1 (SNW1, formerly SKIP) is a highly conserved 536-amino acid spliceosomal protein encoded by a 14-exon gene on chromosome 14, with two known isoforms (20). Initially identified in *Drosophila*, SNW1 harbors a conserved SNW/SKIP domain with the S-N-W-K-N amino acid sequence, and comprises three main regions: N-terminal (residues 1-173), SNW domain (174-232), and the C-terminal (333-536) (21-23). It functions as a transcriptional coactivator in the Notch signaling (24, 25), TGF-β pathway (26), and VDR pathways (27-29).

SNW1 acts as a scaffold protein, facilitating interactions between various spliceosomal components (30, 31). It is involved in the transition from one conformational state of the spliceosome to another one, particularly during the assembly of the catalytic core. When analyzing the protein-protein, protein-RNA, and RNA-RNA interactions within different spliceosomal structures using network theory, *SNW1* displayed high betweenness centrality (32). This suggests that it may serve as a regulatory node during spliceosome activation, bridging the RES complex and NTR complex with its unique role, indicating a potential regulatory function in splicing activation and later stages. *SNW1* is an elongated (non-globular) protein, which allows it to maintain a highly flexible and dynamic state, playing a significant role in network architecture (32, 33). SNW1's interactions with other proteins and RNA elements help stabilize the spliceosome's structure and contribute to its dynamic behavior, influencing the overall architecture and function of the complex (30). Interestingly, SNW1's close interaction partner, PPIL1, a member of the NTC complex, has been increasingly associated with microcephaly-related mutations in recent years (14-16). Here, we report that mutations in *SNW1* impair interactions with core spliceosomal members, disrupt RNA splicing integrity, and result in microcephaly phenotypes in both humans and fruit flies. Our study aims to elucidate the impact of *SNW1* mutations on protein function and their role in the pathogenesis of primary microcephaly. By exploring the molecular mechanisms underlying these mutations, we hope to contribute to a better understanding of the critical role of the spliceosome in brain development and neurodevelopmental disorders.

Results

Identification of Mutations in SNW1

From a cohort of 3699 patients with neurodevelopmental disorders, we identified a *de novo* SNW1 variant in one individual with classic primary microcephaly. Through GeneMatcher, Chigene (Beijing) 's in-house database and the China Epilepsy Gene 1.0 project, nine affected individuals were identified to carry heterozygous variants in *SNW1*, encompassing not only missense variants and microdeletions but also intronic variations (Figure 1A; pathogenic or likely pathogenic (P/LP) variants not directly linked to the clinical phenotype are summarized in Supplementary Table 1). Eight variants were confirmed as *de novo*, while one's inheritance cannot be tested due to adoption.

Except for individual 7, who underwent medical termination at 19 weeks, all presented with overlapping clinical features (Table 1 and Supplementary Table 2). Moderate-to-profound intellectual disability was present in all nine patients, and another most prevalent finding is severe microcephaly, which might be of prenatal onset since five patients with available birth medical data showed small head circumference at birth. Seizures were present in seven individuals, with one (individual 3) developed into epileptic encephalopathy. Additional commonly seen neuropsychiatric manifestations include autism and global developmental delay involving speech, cognition, and motor skills. It is worth noting that most individuals, even the fetus, showed obvious

dysmorphic facial features, including widely spaced teeth, short nose, triangular face, short face, marked prognathism and large ears. Brain MRI results indicated corpus callosum hypoplasia in four individuals and Dandy-Walker malformation in another two. Beyond our study, two previously reported variants within the SNW domain have been linked to neurodevelopmental disorders, reinforcing SNW1's relevance (34). These data reveal a neurodevelopmental syndrome associated with *SNW1 de novo* variants, with core features of severe intellectual disability, microcephaly, brain malformations and facial dysmorphisms.

Patient Mutations Affect SNW1 Function

Among the nine variants identified, three were located at canonical 5' splice donor sites: c.330+2T>C, c.426+1G>A, and c.426+1G>T (Supplementary Figure 1A). These sites, following exons 3 and 4, conform to the conserved GT dinucleotide rule (Supplementary Figure 1B). Multiple in silico splice prediction tools uniformly indicated that all three mutations substantially weaken or abolish the corresponding splice donor sites, likely resulting in exon skipping (Supplementary Table 3), which was validated by minigene splicing assay using the pCAS2 vector (Supplementary Figure 1C). The c.330+2T>C variant generated the wild-type transcript (831 bp) and two aberrant splicing isoforms: one lacking the entire exon 3 (768 bp) and another deleting its last 63 bp (669 bp) (Figure 1B and Supplementary Figure 1D). In contrast, both c.426+1G>A and c.426+1G>T resulted in complete skipping of exon 4 (Figure 1B and Supplementary Figure 1E). Since these losses are multiples of three, the resulting

protein products were identified as D57_K110del, V90_K110del, and V111_E142 del.

The single frameshift variant identified, c.1235_1236insA (F412Lfs17), located in exon 12, introduces a premature termination codon (PTC) in exon 13, predicted to activate the nonsense-mediated mRNA decay (NMD) pathway (Supplementary Figure 1F). To experimentally test this hypothesis, we constructed wild-type and F412Lfs17 mutant vectors encoding SNW1 as a GFP N-terminal fusion protein, and transfected them into HEK293T cells (Supplementary Figure 1G). Cells transfected with *SNW1*-mutated vectors showed reduced fluorescence and protein levels (Figure 1, C and D, Supplementary Figure 1H). Compared to that in SNW1 wild-type cells, SNW1 mRNA expression in the mutated-vector-transfected cells were reduced (Figure 1E). Following cycloheximide treatment to inhibit NMD, SNW1 mRNA levels remained unchanged in wild-type-transfected cells but were significantly elevated in mutant-transfected cells (Figure 1F). These findings demonstrated that the c.1235_1236insA (F412Lfs17) triggers NMD-mediated degradation of the mutant SNW1 mRNA, thereby inhibiting the expression of truncated protein.

To assess the potential functional impact of exon variant-induced residue alterations, we performed a protein sequence alignment of SNW1 orthologs across various species. Protein sequence alignments of *SNW1* revealed that the mutated residues, including G61, G62, A63, D205, and H231, are strictly conserved across multiple species, suggesting that these residues may play a crucial role in maintaining protein function

and evolution (Supplementary Figure 1I). In addition, all amino acid-altering variants were predicted to be intolerant to variation according to MetaDome analysis (Supplementary Figure 1J). To investigate the impact of patient-derived protein variants, we expressed Flag-tagged mutant proteins in HEK293T cells. The results demonstrated that different *SNW1* variants affect protein expression (Figure 1G). G61_G62del and D57_K110del showed decreased expression, D205A exhibited a slight decrease, while M230R H231Y and F412Lfs*17 showed significantly increased expression. No significant changes were observed for the remaining mutants.

SNW1 localizes to the nucleus in a speckled pattern, with its nuclear localization signal (NLS) mapped to the last six C-terminal residue (22, 25, 29, 35-38). For the subcellular localization analysis, the GFP-tagged SNW1 expression plasmid (pEGFP-SNW1) was transfected into HEK293T cells. Confocal microscopy results revealed that the SNW1-EGFP signal was predominantly distributed in a punctate/granular pattern within the nuclei of HEK293T cells (Figure 1H). The majority of the SNW1 mutations did not alter this nuclear localization pattern. In contrast, the F412Lfs*17 SNW1-EGFP mutant was no longer localized to the nucleus but instead displayed a cytosolic distribution, losing its characteristic granular appearance. As a core component of the spliceosome, SNW1 functions continuously from the B complex to the final intron removal (Supplementary Figure 1K). Positioned at the core, SNW1 facilitates the conformational changes of the spliceosome (32), which involves interactions with multiple proteins (Figure 1, I and J). Our mutations are located precisely at these

interfaces, prompting us to consider whether the mutation might affect the stable binding of the protein.

Interactions and Functional Implications of SNW1 Mutations in Spliceosome Complex

The SNW1 does not contain a stably folded domain; rather, it is located in the core region of the splicing complex, functioning like a rope that threads through most of the complex (30). Based on the resolved protein complex structures, we identified that several of our mutations are situated in the interaction regions of SNW1 with other spliceosome components, including PPIL1, PLRG1, and PRPF8 (Figure 1, J and K, Supplementary Figure 1K). We therefore investigated whether these variants disrupt the binding of SNW1 to these proteins. As part of the NTR, SNW1 is incorporated into the spliceosome during the early B^{act} complex stage, and recruits PPIL1 at the mature B complex stage, with the interaction persisting through to the ILS complex after exon excision (Supplementary Figure 1K). Notably, increasing reports have linked *PPIL1* mutations to microcephaly phenotypes, such as the failure of PPIL1 p.R131 to associate with SNW1 (14-16). This further underscores the importance of the interaction between SNW1 and PPIL1 in alternative splicing and disease.

Studies have shown that SNW1 interacts with PPIL1 via electrostatic and hydrophobic forces involving PPIL1's β2-α1, β4-β5, and β7 regions and SNW1 residues 59–79 (23,

33, 39, 40). In this study, three mutations—G61_G62del, A63P, and D57_K110del (deletion of exon 3)—are located at the PPIL1-binding interface. Specifically, analysis of the ILS complex revealed that SNW1 residues GLY62 and ALA63 form hydrogen bonds with ARG131 and ALA95 of PPIL1, respectively (Figure 2A). Co-immunoprecipitation (CoIP) assays using Flag-tagged SNW1 mutants and HA-tagged PPIL1 confirmed that these three variants lost PPIL1 binding, while others remained unaffected (Figure 2B). To further explore the interaction between SNW1 and PPIL1, we examined their subcellular colocalization in three cell lines. PPIL1 alone was distributed evenly in both the nucleus and cytoplasm, with slight nuclear enrichment (Supplementary Figure 2A). However, upon co-expressed with SNW1-WT or other binding-competent SNW1 variants, PPIL1 localization was restricted to the nucleus, suggesting that SNW1 recruits PPIL1 to the spliceosome (Figure 2C and Supplementary 2, B and C). In contrast, coexpression with G61_G62del, A63P, or D57_K110del mutants led to persistent cytoplasmic PPIL1 signals, reflecting their loss of binding. Notably, the F412Lfs*17 mutant retained PPIL1-binding ability but failed to recruit it to the nucleus due to NLS loss, further supporting the regulatory role of SNW1 subcellular localization in determining PPIL1 distribution.

PLRG1, a conserved NTC component, is crucial for alternative splice site selection. In yeast, the interaction between prp45 and prp46 has been confirmed to be essential for pre-mRNA splicing (41). Within the spliceosome, hydrogen bonds are present between SNW1's VAL229 and MET230 and PLRG1's THR369 and ASN370 (Figure 2D). CoIP

results indicate that M230_H231delinsRY enhance the binding with PLRG1 (Figure 2E and Supplementary Figure 2D). For the PLRG1 co-localization analysis, M230_H231delinsRY variant did not exhibit any notable differences from the wild type, and no differences were observed for the other variants except for F412Lfs*17 (Supplementary Figure 2, E-G). The F412Lfs*17 mutant localized exclusively to the cytoplasm, while PLRG1 remained nuclear, suggesting PLRG1 localization is SNW1-independent and not sequentially recruited by SNW1.

For D205A, we observed multiple interactions between residue ASP205 and residues of PRPF8 within the spliceosome complex, including hydrophobic interactions with PHE481 and a salt bridge interaction with HIS121 (Figure 2F). As analyzed, D205A markedly diminishes the binding between SNW1 and PRPF8. (Figure 2G and Supplementary Figure 2H). In summary, all assessed SNW1 patient mutations either affect protein expression or localization, or they influence interactions with other proteins within spliceosome complex. A summary of SNW1 variant types and their experimentally validated effects on splicing, protein expression, and interactions is provided in Supplementary Table 4. These results add value to the notion that these mutations are loss-of-function, which affect the function of the splicing complex and further lead to neurodevelopmental damage.

Assessing the Role of SNW1 in Brain Development Using Drosophila melanogaster

To investigate the in vivo function of SNW1, we used *Drosophila melanogaster*, whose *SNW1* ortholog, *Bx42*, shares 60% amino acid identity, including the important SNW domain (42). To assess the necessity of *Bx42* in neural stem cells, the GAL4-UAS system was used to knock down *Bx42* using RNAi. Male *EGFP* RNAi (control) or *Bx42* RNAi flies were crossed to female *inscuteable-GAL4* (*insc-GAL4*, neural stem cell driver) flies for cell-specific knockdown of *Bx42* in neural stem cells. Third-instar larval brains were dissected and stained with Deadpan (a neural stem cell marker), and brain lobe volume was quantified. The knockdown of *Bx42* in neural stem cells resulted in a significantly reduced brain lobe volume compared to control (Figure 3, A and B, $P = 0.0015$). To ensure that the small brain lobe volume observed was due to the knockdown of *Bx42* transcripts, *Bx42* transcript levels were assessed using qPCR. Ubiquitous knockdown could not be validated since it is embryonic lethal. *Bx42* was knocked down using the neuronal driver neuronal-*Synaptobrevin-GAL4* (*nSyb-GAL4*), as *Bx42* is normally expressed in neurons, and the abundance of neurons compared to neuroblasts makes the detection of knockdown more feasible. We found that the knockdown of *Bx42* resulted in a 55% reduction in the *Bx42* transcript, confirming that RNAi is functioning as expected (Figure 3C).

Using the same crosses and dissection methods described for brain lobe volume, third-instar larval brains were stained with Deadpan and phospho Histone H3 (pHH3) to mark

proliferating neural stem cells. The stereotyped number of neural stem cells in the central brain region of *Drosophila* larvae is around 100 cells, making it easy to quantify and observe changes in cell number (43-46). A significant reduction in the number of neural stem cells in the central brain region was found with *Bx42* knockdown compared to control (Figure 3, D and E, $P < 0.0001$). Additionally, the number of neural stem cells in the central brain region with pHH3 puncta colocalized with Deadpan was counted. Interestingly, while 40% of neural stem cells in controls had positive pHH3 puncta, there was a complete loss of proliferation in central brain neural stem cells with *Bx42* knockdown (Figure 3F, $P < 0.0001$).

To test conservation of protein function between *Drosophila* and humans, *SNW1* cDNA was expressed using the GAL4-UAS system to control expression. The *SNW1* construct is tagged with HA, so to confirm the presence of SNW1 protein, brains were stained for Deadpan and HA. SNW1-HA colocalized with Deadpan, indicating human SNW1 protein is stable in the neural stem cell nucleus as expected (Figure 3G). Flies co-expressing *Luciferase* + *Bx42* RNAi (a GAL4 dilution control) had a significant reduction in brain lobe volume compared to control brains (Figure 3, H and I, $P < 0.0001$), similar to *Bx42* RNAi alone. These results indicate the addition of another UAS construct did not affect knockdown efficiency. Importantly, expression of *SNW1* + *Bx42* RNAi significantly rescued brain lobe volume compared to *Luciferase* + *Bx42* RNAi (Figure 3, H and I, $P = 0.0002$), indicating that human SNW1 and fly *Bx42* are functionally conserved. To verify that expression did not disrupt normal brain

development, human *SNW1* was expressed in neural stem cells of wild type *Drosophila*, and no differences in brain lobe volume were observed (Figure 3J, $P = 0.4495$), indicating no toxic effects. In addition, *Luciferase* + *Bx42* RNAi brains retained reduced neural stem cell number (Figure 3, K and L, $P = 00003$) and a complete absence of proliferation (Figure 3, K and M, $P < 0.0001$), while co-expression of *SNW1* + *Bx42* RNAi rescued both stem cell number (Figure 3, K and L, $P = 0.0121$) and proliferation (Figure 3, K and M, $P < 0.0001$). Together, these results show that fly *Bx42* and human *SNW1* are conserved and both influence brain development.

Impact of *SNW1* Deletion on Proliferation and Apoptosis of Neural Stem Cells in Human Brain Organoids

Since the loss of function of *SNW1* in *Drosophila* results in a microcephaly phenotype similar to that observed in patients, we utilized human embryonic stem cell (hESC)-derived cerebral organoids (hCOs) models to unveil the functions of *SNW1* in human brain development. Analysis of *SNW1* expression patterns in human and mouse fetal brains revealed a pronounced tissue-specific expression during neurodevelopment, with high levels observed in highly proliferating cells and minimal expression in mature neurons (Supplementary Figure 3, A and B). This suggests that SNW1 may play a functional role predominantly during the early stages of neurogenesis, rather than in the maintenance of mature neuronal function. Based on these findings, two heterozygous SNW1 knockout ($SNW1^{+/-}$) hESC lines, designated #1-2 and #2-4, were generated from

H9 hESCs using CRISPR-Cas9 genome editing (Supplementary Figure 3C). Sanger sequencing and PCR electrophoresis confirmed successful heterozygous deletion of exons 4 and 5 in the *SNW1*$^{+/-}$ hESC lines (Supplementary Figure 3, D and E). Subsequent western blot analysis confirmed a significant reduction in *SNW1* expression in both #1-2 and #2-4 lines compared to H9 controls (Supplementary Figure 3F). To further investigate whether the deletion of *SNW1* caused any defects in hESCs, we performed immunostaining and alkaline phosphatase activity assays to check the pluripotency across the three cell lines. The results revealed no significant differences in these markers among the lines, indicating that the expression of core pluripotency markers remained unaffected (Supplementary Figure 3, G-I). The results suggest that *SNW1* deletion did not affect the differentiation potential of hESCs.

After validation of pluripotency by preservation of pluripotency markers, *SNW1*$^{+/-}$ hESCs and H9 cells were further used to generate hCOs (Figure 4A). To determine if the alterations in proliferation observed in fly models could be validated in humans, we measured the sizes of organoids at several time points within 40 days, to trace the possible changes in these organoids (Figure 4B). From day 20, hCOs derived from *SNW1*-KO lines exhibited a significant reduction in size compared to H9 controls, and this smaller volume phenotype persisted as the culture period progressed (Figure 4C). Following this observation, we further investigated the underlying mechanisms causing this developmental difference, focusing on the phenotypic characteristics of neural stem cells (NSCs) in 45-day-old hCOs, as observed in *Drosophila*. The rosette-like structures

within hCOs, which closely resemble the early embryonic neural tube, are primarily composed of NSCs. We used PAX6 as a marker to delineate these structures and identify regions critical for NSC proliferation and differentiation. Quantitative analysis revealed a significant reduction in the area of PAX6+ regions in *SNW1*$^{+/-}$ hCOs compared to controls, suggesting that partial loss of *SNW1* compromises the size of the neural stem cell pool (Figure 4D). To assess the functional state of NSCs within these regions, we performed immunostaining for markers of proliferation (pHH3, Ki67), apoptosis (Caspase3), and neuronal differentiation (MAP2) (Figure 4, E-L). The proportion of cells co-expressing PAX6 and proliferation markers (pHH3 or Ki67) was significantly decreased in *SNW1*$^{+/-}$ organoids, indicating reduced proliferative capacity of NSCs (Figure 4, E, F, I and J). Conversely, the frequency of Caspase3+ cells among the PAX6+ population was markedly increased, suggesting enhanced apoptosis in the absence of sufficient *SNW1* function (Figure 4, G and K). In contrast, the proportion of MAP2+ mature neurons showed no significant difference between *SNW1*$^{+/-}$ and H9 control organoids, reinforcing the notion that SNW1 does not play a major role in the maintenance of differentiated neuronal populations (Figure 4, H and L). Together, these data collectively support a model in which SNW1 is critical for maintaining neural stem cell homeostasis during early neurodevelopment, primarily by sustaining proliferation and inhibiting apoptosis, while not affecting the survival of mature neurons.

SNW1 deficiency leads to widespread transcriptional alterations impacting neuronal differentiation and brain development

As both a transcriptional co-regulator and splicing factor, SNW1 deficiency is highly likely to impact the expression of downstream target genes [192, 273]. To obtain a comprehensive understanding of how *SNW1* haploinsufficiency affects neural progenitor cells (NPCs), we performed bulk RNA sequencing (RNA-seq) analyses on NPCs differentiated for 12 days, and cerebral organoids cultured for 18 and 45 days, derived from both wild-type and $SNW1^{+/-}$ (#1-2) hESCs (Figure 5A). Individual analyses for each group are presented in Supplementary Figure 4-6. Gene Ontology (GO) and KEGG pathway analyses revealed several commonly enriched biological processes and signaling pathways across all three developmental stages, including axonogenesis, forebrain development, the PI3K-Akt signaling pathway, and axon guidance (Figure 5, B and C). Notably, these enrichments were most prominent in 45-day cerebral organoids. Further pathway enrichment analysis using Reactome demonstrated that differentially expressed genes (DEGs) at this stage were predominantly associated with neuronal system (Figure 5D). DisGeNET disease association analysis also revealed notable correlations with neuropsychiatric disorders, further underscoring the pivotal role of SNW1 in neurodevelopment (Figure 5E). Based on these findings, we focused our subsequent analyses on gene expression changes in the 45-day cerebral organoids.

In the 45-day cerebral organoids, we detected 3572 DEGs (|log2FC| > 1 and $P_{adj} < 0.05$), of which 61.99% were upregulated (n=2214) and 38.01% were downregulated (n=1358) (Supplementary Figure 4C). Subsequent functional enrichment analyses revealed that these DEGs are substantially involved in several critical biological processes and signaling pathways, including axonogenesis, forebrain development, apoptotic process, neuroactive ligand−receptor interaction pathway, PI3K−Akt signaling pathway, axon guidance and others (Supplementary Figure 4, D and E). Moreover, genes involved in head development and embryonic morphogenesis, and neurological disorders were also markedly affected (Supplementary Figure 4, F and G). These results indicated that *SNW1* play essential roles in neurodevelopment process, which could be mapped to hCOs development and phenotypes manifestations in *Drosophila* models and patients, especially brain function and neurodevelopment.

Disrupted alternative splicing integrity in *SNW1*$^{+/-}$ human cerebral organoids

To investigate the potential role of *SNW1* in neurodevelopmental disorders associated with primary microcephaly, which is primarily caused by dysfunction in NPCs, we performed transcriptomic analysis and cell cycle assays on NPCs (Supplementary Figure 6). The results demonstrated that haploinsufficiency of *SNW1* (*SNW1*$^{+/-}$) does not affect the NPC cell cycle (Supplementary Figure6, G-I). Transcriptomic profiling revealed that *SNW1* haploinsufficiency predominantly disrupts RNA splicing processes

and alters several signal transduction pathways (Supplementary Figure 6D). However, no enrichment was observed for transcription-related GO terms. Given that SNW1 and PPIL1 exhibit overlapping functions in RNA splicing and display phenotypic similarities, our investigation focuses more on the post-transcriptional regulatory roles of SNW1, particularly its involvement in pre-mRNA splicing regulation.

Comparative splicing analysis was performed using the rMATS pipeline between the two groups, revealing a total of 4896 significant alternative splicing (AS) events. Notably, skipped exon (SE) events represented the majority, accounting for 69.77% of the total (Figure 6A and Supplementary Figure 7, A and B). The markedly high frequency of SEs (1970/1446) observed in *SNW1*-KO hCOs stands out compared to other observed AS events ratios, while no significant difference was detected in retained intron (RI) events (Figure 6B). Compared to the control group, SE events in *SNW1*-KO hCOs exhibit a significant increase in the length of skipped exons, indicating that SNW1 deficiency induces aberrant splicing at longer exons (Figure 6C). There was no discernible difference in the preference for 5' and 3' splice sites among SE events (Supplementary Figure 7, C and D). SE and RI events are mediated by distinct molecular mechanisms involving the exon junction complex (EJC) pathways. The detection of SE defects suggests a regulatory role of SNW1 in a specific subset of splicing events. Furthermore, the SE events were particularly enriched in genes with a longer isoform and a higher number of isoforms, which we refer to as exon skipping genes (ESGs) (Figure 6 D and E). Alternative splicing is highly prevalent and strictly

conserved in the brain, contributing to the specificity and diversity of neural circuits, thereby resulting in genes with longer and more numerous isoforms (17, 18, 47, 48). These characteristics of ESGs also imply that *SNW1* deficiency renders the brain more susceptible compared to other tissues. Profiling of ESGs identified axon development as the most significantly disrupted module, reinforcing the phenotypes observed in flies and patients (Supplementary Figure 7, E and F).

During the mRNA processing in the presence of *SNW1* deficiency, SE splicing may lead to alterations in isoform ratios or destabilization of mRNA, thereby impacting gene expression. Among the 3,572 DEGs, 235 exhibited exon skipping (Figure 6F). Likewise, downregulated DEGs in *SNW1*-KO hCOs are significantly enriched for long genes, with an average of fewer than 8 annotated isoforms (Figure 6, G and H). These findings suggest that SNW1 is crucial for the proper spliceosomal processing of long mRNAs that are highly expressed in the brain. To validate our bioinformatics analysis, inclusion patterns of SE events in selected DEGs were validated by RT-qPCR (Supplementary Figure 8). Due to their roles in neurodevelopmental disorders, we selected 11 candidate genes from the 235 genes identified, which are associated with neurodevelopmental disorders or microcephaly according to the DisGeNET database. The results demonstrated that the overall mRNA levels of these genes in *SNW1*-KO hCOs changed significantly, as expected. For the SE events, primers were designed to measure the ratio of exon-included mRNA to the total mRNA, showing that most exhibited exon skipping (Supplementary Figure 8 B-I). This exon loss may result from aberrant

splicing or the selection of non-canonical transcript isoforms, potentially explaining some of the observed differences in gene expression.

Among these genes, we selected three representative ones, all of which have been confirmed to be associated with neurodevelopment—*CENPE*, *MEF2C*, and *NRXN2* (Figure 6, I-K and Supplementary Figure 9). For *CENPE*, there are currently two validated transcripts, with SE occurring in exon 38 of the canonical transcript (Figure 6, I-K). Similarly, in *SNW1*$^{+/-}$ brains, exon 8 of the canonical transcript of *MEF2C* was skipped, whereas the canonical transcript represents the longest isoform (Supplementary Figure 9, A-C). Additionally, there were instances such as *NRXN2*, where multiple SE events occurred (Supplementary Figure 9, D-F). Based on bioinformatics analysis and qPCR validation, this was also attributed to differences in transcript selection between the two groups. Collectively, these findings indicate that *SNW1* deficiency compromises splicing fidelity, leading to substantial changes in splicing patterns and expression levels of genes critical for brain and neural development.

Discussion

In this study, we identified nine *SNW1* variants in individuals with NDDs accompanied by primary microcephaly, suggesting *SNW1* as a potential candidate gene for NDDs. Mechanistically, a series of in vitro functional assays supported the pathogenicity of these variants by demonstrating loss of *SNW1* function. The observed dysfunction was found to impair RNA splicing fidelity, suppress neural stem cell proliferation, and induce apoptosis, ultimately contributing to a significant reduction in brain volume. These findings underscore the critical role of spliceosome integrity in neurodevelopment and highlight the importance of accurate splicing in neural development.

SNW1, a conserved component of the NTC, has been rarely studied in the context of neurodevelopment process. Here, through rigorous patient recruitment and variant screening, we identified a spectrum of *SNW1* variants in NDD patients, including start codon disruptions, missense mutations, splice-site variants, and frameshift mutations. Despite their heterogeneity, the affected individuals exhibited overlapping clinical phenotypes, suggesting a shared pathogenic mechanism, likely mediated by splicing dysfunction. Functional analyses encompassing transcript processing, protein interaction, and subcellular localization provided direct evidence for the pathogenicity of these *SNW1* variants. However, given the rarity of these mutations, we cannot fully exclude the possibility that some variants are merely rare variants observed in the population. Additionally, the limited sample size constrained the statistical power for

robust genotype–phenotype correlation analyses. Therefore, further validation in larger and independent cohorts is essential to establish the pathogenic relevance of these *SNW1* mutations in microcephaly. Moreover, the presence of epilepsy and autism spectrum behaviors in affected individuals raises the possibility that *SNW1* variants may disrupt neuronal network formation and function, leading to abnormalities in electrophysiological activity and synaptic plasticity. These clinical features align with SNW1's core role in the spliceosome, where aberrant RNA splicing can dysregulate genes essential for neuronal differentiation, migration, and synapse formation(49, 50). While this hypothesis is supported by previous literature, it remains to be directly tested and represents a key direction for future research.

Then, to explore potential biological mechanisms underlying *SNW1* deficiency in NDDs, we established *SNW1* knockdown models in *Drosophila* and cerebral organoids. Knockdown of the *SNW1* ortholog *Bx42* in *Drosophila* impaired central nervous system development, marked by reduced brain lobe size and loss of neural stem cell proliferation. Notably, these phenotypes were rescued by reintroduction of human *SNW1*, indicating conserved function. Due to the lack of patient-derived cells, our study utilized a heterozygous knockout model based on hESCs, which may overlook patient-specific genetic modifiers. In cerebral organoids, *SNW1* haploinsufficiency recapitulated the microcephaly phenotype, characterized by impaired neural progenitor proliferation, increased apoptosis, and disrupted splicing of key neurodevelopmental genes. These observations underscore the fundamental role of neurogenesis—

comprising proliferation, migration, and differentiation of neural stem cells—in cortical development (51). Perturbations in progenitor cell proliferation or apoptosis during neurogenesis often lead to changes in brain size (52). Beyond organoid and *Drosophila* models, *SNW1* knockdown also leads to smaller head structures and less developed forebrains in *Xenopus* embryos and zebrafish, indicating evolutionarily conserved roles in early brain formation (22, 53). However, it is important to recognize limitations in model fidelity. *Drosophila* lacks mammalian brain architecture and circuits involved in higher cognition, while organoids lack vascularization, immune microenvironments, and long-term maturation required to study processes like synaptic pruning or myelination. Future research using patient-derived iPSCs or non-human primate models, combined with genome editing technologies, will allow us to introduce precise *SNW1* variants in endogenous contexts and further elucidate disease mechanisms.

Transcriptomic analysis of *SNW1*$^{+/-}$ hCOs revealed widespread RNA splicing dysregulation, with notable enrichment of aberrant splicing events in genes essential for neurodevelopment (54). Previous research has also shown that deletion of SNW1 leads to rapid downregulation of p21 and renders cells more susceptible to p53-mediated apoptosis (31, 55). Our results demonstrated alternative splicing defects were particularly evident in genes like CENPE and MEF2C. *CENPE* primarily participates in precise chromosome segregation, kinetochore microtubule attachment, and mitotic checkpoint control. Defects in *CENPE* can lead to abnormal division of neural progenitor cells during development, identified previously as pathogenic in primary

microcephaly (56, 57). Meanwhile, *MEF2C* is crucial for cardiac muscle formation and neuronal development and function. Research has linked *MEF2C* deficiency syndrome to moderate to severe intellectual disability, epilepsy, and language impairment, validated in animal models (58). Transcriptomic profiling identified ESG as significantly enriched in axonal development, consistent with previous reports (18, 59). While our study connected spliceosomal defects with NDD pathogenesis, further experiments are required to validate causal relationships. It remains to be determined whether observed phenotypes are driven by specific mis-spliced genes such as *MEF2C* or *CENPE*, or if compensatory mechanisms attenuate splicing defects in vivo. Notably, some variants (e.g., Met1?) are predicted to abrogate translation initiation entirely, yet patients carrying these mutations do not show significantly different phenotypes from those with other variants. This raises the possibility of residual truncated protein expression or compensatory upregulation of *SNW1* paralogs, which may buffer the splicing defect and explain the partial discordance between molecular anomalies and clinical severity. Future efforts should focus on spatiotemporal analysis of splicing disruptions in patient-derived neural precursor cells, to map dynamic effects and understand functional consequences.

Global splicing analysis further revealed that SNW1 deficiency particularly enriched skipped exon (SE) events in long transcripts and genes with multiple isoforms. The developing brain expresses longer genes and exhibits highly active alternative splicing, relying on a sophisticated splicing regulatory network to ensure precise expression of

neural-specific isoforms. The observed exon-skipping (SE) events can result in either truncated mRNAs that escape nonsense-mediated decay or isoform ratio imbalances that destabilize gene function. The observed SE events can result in either truncated mRNAs that escape nonsense-mediated decay or isoform ratio imbalances that destabilize gene function. However, these findings are limited by current transcript annotation databases, which have low 5′ and 3′ end coverage, especially for long or low-abundance transcripts. To overcome these limitations, we plan to implement long-read sequencing and single-cell transcriptomics to delineate full-length transcript isoforms and splicing heterogeneity in neural progenitors. Targeted validation using RACE-PCR will also be employed to confirm key splicing events. These technologies will enhance the precision of differential splicing analysis and facilitate more accurate genotype–phenotype correlations.

Importantly, our findings place SNW1 within a broader context of spliceosomal components implicated in NDDs. For instance, *SF3B1* mutations cause skeletal abnormalities, while *SF3B4* mutations lead to Nager syndrome (60, 61). Similarly, *EFTUD2* mutations result in mandibulofacial dysostosis with microcephaly (11, 12), and mutations in *PPIL1*, *PRP17*, and *PRPF19* are linked to neurodegenerative pontocerebellar hypoplasia (2, 14, 15). Notably, SNW1 deficiency shares overlapping phenotypes with PPIL1 and PRPF9 mutant patients, suggesting a core role of the NTC complex. Transcriptomic data suggest that spliceosomal mutations often exhibit locus-specific effects on splice site recognition, altering mRNA isoform diversity and

contributing to distinct clinical phenotypes (62).The electron microscopy structure of the human spliceosome reveals that *SNW1* is essential for spliceosome function, especially exhibiting betweenness centrality within the B^{act} complex and ILS (30, 32, 63, 64). SNW1 is located in the core region of the spliceosome, functioning similarly to a thread woven through its components. Several *SNW1* mutations have been identified in the interaction regions between SNW1 and spliceosome components such as PPIL1, PLRG1, and PRPF8, highlighting the regulatory role of *SNW1* within the spliceosome. Three mutations presented in this study demonstrate a complete loss of interaction with PPIL1. Although yeast and human spliceosomes share a set of evolutionarily conserved core spliceosomal proteins, human spliceosomal proteins often contain additional unstructured regions. The most important difference between them is the presence of the RNA helicase Aquarius and peptidyl prolyl isomerases (30). These findings emphasize the critical role of SNW1-PPIL1 interactions in splicing regulation and disease pathology.

Additionally, haploinsufficiency of *SNW1* was found to alter multiple signaling pathways beyond splicing. Previous studies in *Xenopus* and zebrafish have suggested that SNW1 may function as a scaffold in β-catenin/TCF-mediated transcription, thereby regulating early neurodevelopmental factors such as SOX3, SNAI2, and EN2 (22, 53). SNW1 has also been implicated in Notch, BMP, and Wnt signaling during early embryogenesis (65-68). Therefore, it is plausible that SNW1 dosage affects signal transduction directly or indirectly through splicing perturbations. Further mechanistic

studies are necessary to disentangle these interrelated effects.

In conclusion, our study elucidates the critical role of SNW1 in spliceosome function and its potential impact on neurodevelopmental disorders. By providing insights into the molecular mechanisms underlying *SNW1*-related neurodevelopmental disorders, our research may pave the way for potential therapeutic strategies targeting spliceosomal function.

Methods

The detailed materials and methods are provided in the Supplemental Materials

Sex as a biological variable.

Sex was not evaluated as a biological variable. Both male and female flies were used in this study.

Fly Stocks

The Drosophila strains were obtained from the Drosophila Genomics Resource Center. The following fly lines were used: *Bx42* (the Drosophila homolog of *SNW1*) RNAi *(P{TRiP.HMC00086}attP40)*, *EGFP* RNAi *(P{VALIUM22-EGFP.shRNA.attP40)*, inscuteable-*GAL4 (P{w[+mW.hs]=GawB}insc[Mz1407]), neuronal Synaptobrevin-GAL4 (P{y[+t7.7] w[+mC]=nSyb-GAL4.P}attP2), UAS-Luciferase, P{UAS-SNW1-HA}VK37* (69, 70). All flies were maintained at 25°C and grown on Archon glucose formula food in medium, wide plastic vials. RNAi crosses were set at 29°C and grown on Archon glucose formula food with bromophenol blue added. Brain volume measurements and proliferation assessments were performed on wandering third-instar larval brains. The wandering third-instar larval stage was identified morphologically by extruding spiracles and gut clearance (71, 72).

Cell culture

HEK293T, HEK293, and Hela cells were obtained from Cell Bank, Chinese Academy of Sciences. HEK293T, HEK293, and Hela cells were cultured in high-glucose

Dulbecco's Modified Eagle Medium (DMEM) (Gibco, Cat. No: C11995500BT) supplemented with 10% FBS (Gibco, Cat. No: 10091148) and 1% penicillin-streptomycin (Beyotime, Cat. No: C0222). Feeder-free cells were cultured in mTeSR medium (Stemcell Technologies) with Matrigel (Corning). Feeder dependent H9 hESCs were cultured on CF1-c-irradiated mouse embryonic fibroblasts with hESC medium containing DMEM/F12 (Gibco), 0.5% GlutaMax (Gibco), 20% KnockOut serum replacement (KSOR, Gibco), 1% Non-Essential Amino Acids Solution (MEM-NEAA, Gibco), and 0.1 mM b-mercaptoethanol (Amresco), with additional freshly added 4 ng/ml bFGF (Sino Biological). Detailed procedures were previously described (73).

Generation of human embryonic stem cell-derived cerebral organoids

The H9 human embryonic stem cell (hESC) line used in this study was preserved from laboratory stocks. The *SNW1* knockout cell line was constructed in H9 hESCs using CRISPR-Cas9 gene editing technology. To delete *SNW1*, two guide RNAs targeting the introns flanking exon 4 and exon 5 were designed and cloned into plasmids, which were then transfected into H9 hESCs via the Neon Transfection system (Invitrogen). Through homologous recombination, eGFP replaced exon 4 and exon 5 of SNW1, and GFP^+ *SNW1*-KO cells (heterozygous) were identified by FACS.

hESCs-derived cerebral organoids (hCOs) were established following the protocol

published by Lancaster (74). H9 hESC or *SNW1*-KO cells were treated with EDTA and Accutase to form single-cell solutions to generate embryoid body (EB). Then, 9000 cells were plated into each well of a low-binding 96-well plate in mTeSR medium with ROCK inhibitors (Selleck). After three days, fresh mTeSR without ROCK inhibitors was added. On day five, EBs were transferred to neural induction media, which was refreshed every two days for six days. The neural induction media consisted of DMEM/F-12 (Gibco) supplemented with 1% N2 Supplement (Gibco), 1% L-GlutaMAX (Thermo), 1% MEM-NEAA (Gibco), 0.01% heparin solution. Subsequently, EBs were embedded in Matrigel droplets and cultured in differentiation medium without vitamin A. The differentiation medium consisted of 50% DMEM/F-12 (1:1) and 50% Neurobasal supplemented with 1% N2 Supplement, 1% B27 Supplement minus Vitamin A, 1% GlutaMAX, 1% MEM-NEAA, 0.1 mM β-mercaptoethanol, 20 ng/mL EGF (Epidermal Growth Factor), and 20 ng/mL FGF-2. After 10 days, droplets were transferred to a medium with vitamin A on an orbital shaker. Media were changed every 7 days, and the morphological appearance of organoids in both groups was examined.

Statistical analysis

All power analyses were done with the G*Power program post-hoc to assess the power of our n sizes. Since all analyses being assessed were independent t-tests we used the same parameters for assessing power and only substituted the appropriate means and standard deviations. The following settings were used: t tests were selected for test

family and “Means: Difference between two independent means (two groups)”. We selected a two-tailed test and left the preset alpha level at 0.05.

Study approval

The patients included in this study were from seven unrelated families, originating from various regions around the world, including China, France, Germany, and America. Information regarding gender, age, and health status is listed in the supplementary Table 1 and 2. All work involving patients was approved by the ethics committee of the Maternal and Child Health Hospital of Hunan Province (2024-S043) and conducted in accordance with established guidelines. Consent forms were signed by all patients or their guardians, explicitly permitting the use of the patients' photographs in this study.

Data availability

The raw sequence data reported in this paper have been deposited in the Genome Sequence Archive in National Genomics Data Center, China National Center for Bioinformation / Beijing Institute of Genomics, Chinese Academy of Sciences (GSA-Human: HRA012051 and HRA008110) that are publicly accessible at https://ngdc.cncb.ac.cn/gsa-human. All underlying numerical data used to generate the graphs and statistical analyses in this study are provided in the Supporting Data Values file.

Author contributions

The number of experiments performed by each researcher was the method used for assigning the order of the three co–first authors. Lei Ji led the molecular experiments and manuscript writing, with Keyi Li, Zhen Liu, Decheng Ren, Ke Yang, Yingying Luo, and Fengping Yang providing assistance. Jin Yan and Jing Xu conducted the organoid-related experiments, with support from Zhenming Guo, Gui Wang, zhenglong Xiang, Yuan Wang, Huaizhe Zhan, and Shan Bian. Nicole A. Losurdo performed the *Drosophila* experiments, assisted by Adriana Bibo and Nichole Link. Hua Wang and Liangjie Liu were responsible for the bioinformatics analysis. The remaining authors contributed to providing and analyzing the clinical data of patients. The corresponding authors, Shan Bian, Guang He, and Xiao Mao supervised the project design and revisions to the manuscript.

Acknowledgements

We extend our sincere appreciation to the authors and laboratories who made this work possible. We are thankful to the patients and their families for their participation in this research project. We thank the databases of Chigene (Beijing)' inhouse database, Gene4denovo, GeneMatcher, China Epilepsy Gene V.1.0 and their contributors for providing these valuable public datasets. This project is supported by the National Key Research and Development Program (2024YFC2707002, 2020YFA0112500, 2021YFA1100400), Innovation Program of Shanghai Municipal Education Commission (2023ZKZD16), the National Natural Science Foundation of China (82071262, 32300464, 32271019), Natural Science Foundation of Shanghai (20ZR1427200, 20511101900, 21ZR1433000, 22ZR1462600), Shanghai Municipal Science and Technology Major Project (20JC1418600), the Shanghai Leading Academic Discipline Project (B205), China Postdoctoral Science Foundation (2023M732266), the Major Scientific and Technological Projects for Collaborative Prevention and Control of Birth Defects in Hunan Province (2019SK1010, 2019SK1014), Natural Science Foundation of Hunan Province (2022JJ40206), Ruixin project of Hunan Provincial Maternal and Child Health Care Hospital (2023RX01), Key Technology Breakthrough Program of Ningbo Sci-Tech Innovation YONGJIANG 2035 (2024Z221), Municipal Public Welfare Project (2022S035), Jiangxi Provincial Department of Science and Technology (20203BBGL73132), Shanghai Jiao Tong University STAR Grant (YG2023ZD26, YG2023LC14), and NSF GRFP (2139322).

Competing interests

The authors have declared that no conflict of interest exists.

References

1. Daguenet E, Dujardin G, and Valcarcel J. The pathogenicity of splicing defects: mechanistic insights into pre-mRNA processing inform novel therapeutic approaches. *EMBO Rep.* 2015;16(12):1640-55.
2. Li D, Wang Q, Bayat A, Battig MR, Zhou Y, Bosch DG, et al. Spliceosome malfunction causes neurodevelopmental disorders with overlapping features. *J Clin Invest.* 2024;134(1).
3. Wahl MC, Will CL, and Luhrmann R. The spliceosome: design principles of a dynamic RNP machine. *Cell.* 2009;136(4):701-18.
4. Shi YG. Mechanistic insights into precursor messenger RNA splicing by the spliceosome. *Nat Rev Mol Cell Bio.* 2017;18(11):655-70.
5. Makarova OV, Makarov EM, Urlaub H, Will CL, Gentzel M, Wilm M, et al. A subset of human 35S U5 proteins, including Prp19, function prior to catalytic step 1 of splicing. *EMBO J.* 2004;23(12):2381-91.
6. Hogg R, McGrail JC, and O'Keefe RT. The function of the NineTeen Complex (NTC) in regulating spliceosome conformations and fidelity during pre-mRNA splicing. *Biochem Soc Trans.* 2010;38(4):1110-5.
7. Chanarat S, and Strasser K. Splicing and beyond: the many faces of the Prp19 complex. *Biochim Biophys Acta.* 2013;1833(10):2126-34.
8. Fu X, Kaur H, Rodgers ML, Montemayor EJ, Butcher SE, and Hoskins AA. Identification of transient intermediates during spliceosome activation by single molecule fluorescence microscopy. *Proc Natl Acad Sci U S A.* 2022;119(48):e2206815119.
9. Fica SM, and Nagai K. Cryo-electron microscopy snapshots of the spliceosome: structural insights into a dynamic ribonucleoprotein machine. *Nat Struct Mol Biol.* 2017;24(10):791-9.
10. Mao H, McMahon JJ, Tsai YH, Wang Z, and Silver DL. Haploinsufficiency for Core Exon Junction Complex Components Disrupts Embryonic Neurogenesis and Causes p53-Mediated Microcephaly. *PLoS Genet.* 2016;12(9):e1006282.
11. Lines MA, Huang L, Schwartzentruber J, Douglas SL, Lynch DC, Beaulieu C, et al. Haploinsufficiency of a spliceosomal GTPase encoded by EFTUD2 causes mandibulofacial dysostosis with microcephaly. *Am J Hum Genet.* 2012;90(2):369-77.

12. Jacob A, Pasquier J, Carapito R, Aurade F, Molitor A, Froguel P, et al. A de novo synonymous variant in EFTUD2 disrupts normal splicing and causes mandibulofacial dysostosis with microcephaly: case report. *BMC Med Genet.* 2020;21(1):182.

13. Engal E, Oja KT, Maroofian R, Geminder O, Le TL, Marzin P, et al. Bi-allelic loss-of-function variants in WBP4, encoding a spliceosome protein, result in a variable neurodevelopmental syndrome. *Am J Hum Genet.* 2023.

14. Chai G, Webb A, Li C, Antaki D, Lee S, Breuss MW, et al. Mutations in Spliceosomal Genes PPIL1 and PRP17 Cause Neurodegenerative Pontocerebellar Hypoplasia with Microcephaly. *Neuron.* 2021;109(2):241-56 e9.

15. Abdel-Salam GMH, and Abdel-Hamid MS. A founder PPIL1 variant underlies a recognizable form of microlissencephaly with pontocerebellar hypoplasia. *Clin Genet.* 2023;104(3):356-64.

16. Zhang Y, Yan L, Xie M, Xue J, Yang X, Xue Y, et al. Report of new variants in PPIL1 underlying type 14 pontocerebellar hypoplasia and their associated phenotypic manifestations in two fetuses. *Am J Med Genet A.* 2023;191(8):2193-7.

17. Li Q, Lee JA, and Black DL. Neuronal regulation of alternative pre-mRNA splicing. *Nat Rev Neurosci.* 2007;8(11):819-31.

18. Raj B, and Blencowe BJ. Alternative Splicing in the Mammalian Nervous System: Recent Insights into Mechanisms and Functional Roles. *Neuron.* 2015;87(1):14-27.

19. Staley JP, and Guthrie C. Mechanical devices of the spliceosome: motors, clocks, springs, and things. *Cell.* 1998;92(3):315-26.

20. Neubauer G, King A, Rappsilber J, Calvio C, Watson M, Ajuh P, et al. Mass spectrometry and EST-database searching allows characterization of the multi-protein spliceosome complex. *Nat Genet.* 1998;20(1):46-50.

21. Saumweber H, Frasch M, and Korge G. Two puff-specific proteins bind within the 2.5 kb upstream region of the Drosophila melanogaster Sgs-4 gene. *Chromosoma.* 1990;99(1):52-60.

22. Wang Y, Fu Y, Gao L, Zhu G, Liang J, Gao C, et al. Xenopus skip modulates Wnt/beta-catenin signaling and functions in neural crest induction. *J Biol Chem.* 2010;285(14):10890-901.

23. Folk P, Puta F, and Skruzny M. Transcriptional coregulator SNW/SKIP: the concealed tie of dissimilar pathways. *Cell Mol Life Sci.* 2004;61(6):629-40.

24. Zhou S, Fujimuro M, Hsieh JJ, Chen L, and Hayward SD. A role for SKIP in EBNA2 activation

of CBF1-repressed promoters. *J Virol.* 2000;74(4):1939-47.

25. Zhang J, Chen H, Weinmaster G, and Hayward SD. Epstein-Barr virus BamHi-a rightward transcript-encoded RPMS protein interacts with the CBF1-associated corepressor CIR to negatively regulate the activity of EBNA2 and NotchIC. *J Virol.* 2001;75(6):2946-56.

26. Leong GM, Subramaniam N, Figueroa J, Flanagan JL, Hayman MJ, Eisman JA, et al. Ski-interacting protein interacts with Smad proteins to augment transforming growth factor-beta-dependent transcription. *J Biol Chem.* 2001;276(21):18243-8.

27. Baudino TA, Kraichely DM, Jefcoat SC, Jr., Winchester SK, Partridge NC, and MacDonald PN. Isolation and characterization of a novel coactivator protein, NCoA-62, involved in vitamin D-mediated transcription. *J Biol Chem.* 1998;273(26):16434-41.

28. MacDonald PN, Baudino TA, Tokumaru H, Dowd DR, and Zhang C. Vitamin D receptor and nuclear receptor coactivators: crucial interactions in vitamin D-mediated transcription. *Steroids.* 2001;66(3-5):171-6.

29. Zhang C, Dowd DR, Staal A, Gu C, Lian JB, van Wijnen AJ, et al. Nuclear coactivator-62 kDa/Ski-interacting protein is a nuclear matrix-associated coactivator that may couple vitamin D receptor-mediated transcription and RNA splicing. *J Biol Chem.* 2003;278(37):35325-36.

30. Haselbach D, Komarov I, Agafonov DE, Hartmuth K, Graf B, Dybkov O, et al. Structure and Conformational Dynamics of the Human Spliceosomal B Complex. *Cell.* 2018;172(3):454-+.

31. Sato N, Maeda M, Sugiyama M, Ito S, Hyodo T, Masuda A, et al. Inhibition of SNW1 association with spliceosomal proteins promotes apoptosis in breast cancer cells. *Cancer Med.* 2015;4(2):268-77.

32. Kaur H, van der Feltz C, Sun Y, and Hoskins AA. Network theory reveals principles of spliceosome structure and dynamics. *Structure.* 2022;30(1):190-200 e2.

33. Wang X, Zhang S, Zhang J, Huang X, Xu C, Wang W, et al. A large intrinsically disordered region in SKIP and its disorder-order transition induced by PPIL1 binding revealed by NMR. *J Biol Chem.* 2010;285(7):4951-63.

34. Kaplanis J, Samocha KE, Wiel L, Zhang Z, Arvai KJ, Eberhardt RY, et al. Evidence for 28 genetic disorders discovered by combining healthcare and research data. *Nature.* 2020;586(7831):757-62.

35. Mintz PJ, Patterson SD, Neuwald AF, Spahr CS, and Spector DL. Purification and biochemical

characterization of interchromatin granule clusters. *EMBO J.* 1999;18(15):4308-20.

36. Li Y, Xia C, Feng J, Yang D, Wu F, Cao Y, et al. The SNW Domain of SKIP Is Required for Its Integration into the Spliceosome and Its Interaction with the Paf1 Complex in Arabidopsis. *Mol Plant.* 2016;9(7):1040-50.

37. Kim YJ, Noguchi S, Hayashi YK, Tsukahara T, Shimizu T, and Arahata K. The product of an oculopharyngeal muscular dystrophy gene, poly(A)-binding protein 2, interacts with SKIP and stimulates muscle-specific gene expression. *Hum Mol Genet.* 2001;10(11):1129-39.

38. Guo Y, Yang Y, Huang Y, and Shen HB. Discovering nuclear targeting signal sequence through protein language learning and multivariate analysis. *Anal Biochem.* 2020;591:113565.

39. Xu C, Zhang J, Huang X, Sun J, Xu Y, Tang Y, et al. Solution structure of human peptidyl prolyl isomerase-like protein 1 and insights into its interaction with SKIP. *J Biol Chem.* 2006;281(23):15900-8.

40. Stegmann CM, Luhrmann R, and Wahl MC. The crystal structure of PPIL1 bound to cyclosporine A suggests a binding mode for a linear epitope of the SKIP protein. *PLoS One.* 2010;5(4):e10013.

41. Albers M, Diment A, Muraru M, Russell CS, and Beggs JD. Identification and characterization of Prp45p and Prp46p, essential pre-mRNA splicing factors. *RNA.* 2003;9(1):138-50.

42. Dahl R, Wani B, and Hayman MJ. The Ski oncoprotein interacts with Skip, the human homolog of Drosophila Bx42. *Oncogene.* 1998;16(12):1579-86.

43. Rolls MM, Albertson R, Shih HP, Lee CY, and Doe CQ. Drosophila aPKC regulates cell polarity and cell proliferation in neuroblasts and epithelia. *J Cell Biol.* 2003;163(5):1089-98.

44. Lee CY, Andersen RO, Cabernard C, Manning L, Tran KD, Lanskey MJ, et al. Drosophila Aurora-A kinase inhibits neuroblast self-renewal by regulating aPKC/Numb cortical polarity and spindle orientation. *Genes Dev.* 2006;20(24):3464-74.

45. Lee CY, Robinson KJ, and Doe CQ. Lgl, Pins and aPKC regulate neuroblast self-renewal versus differentiation. *Nature.* 2006;439(7076):594-8.

46. Lee CY, Wilkinson BD, Siegrist SE, Wharton RP, and Doe CQ. Brat is a Miranda cargo protein that promotes neuronal differentiation and inhibits neuroblast self-renewal. *Dev Cell.* 2006;10(4):441-9.

47. Patowary A, Zhang P, Jops C, Vuong CK, Ge X, Hou K, et al. Developmental isoform diversity

in the human neocortex informs neuropsychiatric risk mechanisms. *Science.* 2024;384(6698):eadh7688.

48. Lipscombe D, and Lopez Soto EJ. Alternative splicing of neuronal genes: new mechanisms and new therapies. *Curr Opin Neurobiol.* 2019;57:26-31.

49. Zhou Y, Song H, and Ming G-L. Genetics of human brain development. *Nat Rev Genet.* 2024;25(1):26-45.

50. Farcy S, Albert A, Gressens P, Baffet AD, and El Ghouzzi V. Cortical Organoids to Model Microcephaly. *Cells.* 2022;11(14).

51. Zhou Y, Song H, and Ming GL. Genetics of human brain development. *Nat Rev Genet.* 2024;25(1):26-45.

52. Jayaraman D, Bae BI, and Walsh CA. The Genetics of Primary Microcephaly. *Annu Rev Genom Hum G.* 2018;19:177-200.

53. Wu MY, Ramel MC, Howell M, and Hill CS. SNW1 is a critical regulator of spatial BMP activity, neural plate border formation, and neural crest specification in vertebrate embryos. *PLoS Biol.* 2011;9(2):e1000593.

54. Beusch I, Rao B, Studer MK, Luhovska T, Sukyte V, Lei S, et al. Targeted high-throughput mutagenesis of the human spliceosome reveals its in vivo operating principles. *Mol Cell.* 2023;83(14):2578-94 e9.

55. Chen Y, Zhang L, and Jones KA. SKIP counteracts p53-mediated apoptosis via selective regulation of p21Cip1 mRNA splicing. *Genes Dev.* 2011;25(7):701-16.

56. Mirzaa GM, Vitre B, Carpenter G, Abramowicz I, Gleeson JG, Paciorkowski AR, et al. Mutations in CENPE define a novel kinetochore-centromeric mechanism for microcephalic primordial dwarfism. *Hum Genet.* 2014;133(8):1023-39.

57. Fang H, Zhang Y, Lin C, Sun Z, Wen W, Sheng H, et al. Primary microcephaly gene CENPE is a novel biomarker and potential therapeutic target for non-WNT/non-SHH medulloblastoma. *Front Immunol.* 2023;14:1227143.

58. Harrington AJ, Bridges CM, Berto S, Blankenship K, Cho JY, Assali A, et al. MEF2C Hypofunction in Neuronal and Neuroimmune Populations Produces MEF2C Haploinsufficiency Syndrome-like Behaviors in Mice. *Biol Psychiatry.* 2020;88(6):488-99.

59. Furlanis E, and Scheiffele P. Regulation of Neuronal Differentiation, Function, and Plasticity

by Alternative Splicing. *Annu Rev Cell Dev Biol.* 2018;34:451-69.

60. Kfir N, Lev-Maor G, Glaich O, Alajem A, Datta A, Sze SK, et al. SF3B1 association with chromatin determines splicing outcomes. *Cell Rep.* 2015;11(4):618-29.

61. Bernier FP, Caluseriu O, Ng S, Schwartzentruber J, Buckingham KJ, Innes AM, et al. Haploinsufficiency of SF3B4, a component of the pre-mRNA spliceosomal complex, causes Nager syndrome. *Am J Hum Genet.* 2012;90(5):925-33.

62. Chen M, and Manley JL. Mechanisms of alternative splicing regulation: insights from molecular and genomics approaches. *Nat Rev Mol Cell Biol.* 2009;10(11):741-54.

63. Zhang XF, Yan CY, Zhan XC, Li LJ, Lei JL, and Shi YG. Structure of the human activated spliceosome in three conformational states. *Cell Res.* 2018;28(3):307-22.

64. Fica SM, Oubridge C, Wilkinson ME, Newman AJ, and Nagai K. A human postcatalytic spliceosome structure reveals essential roles of metazoan factors for exon ligation. *Science.* 2019;363(6428):710-4.

65. Hong M, He J, and Li S. SNW1 regulates Notch signaling in neuroblastoma through interacting with RBPJ. *Biochem Biophys Res Commun.* 2019;509(4):869-76.

66. Figueroa JD, and Hayman MJ. Differential effects of the Ski-interacting protein (SKIP) on differentiation induced by transforming growth factor-beta1 and bone morphogenetic protein-2 in C2C12 cells. *Exp Cell Res.* 2004;296(2):163-72.

67. She C, Zhu J, Liu A, Xu Y, Jiang Z, and Peng Y. Dexmedetomidine Inhibits NF-κB-Transcriptional Activity in Neurons Undergoing Ischemia-Reperfusion by Regulating O-GlcNAcylation of SNW1. *Journal of Neuropathology & Experimental Neurology.* 2022;81(10):836-49.

68. Verma S, De Jesus P, Chanda SK, and Verma IM. SNW1, a Novel Transcriptional Regulator of the NF-kappaB Pathway. *Mol Cell Biol.* 2019;39(3):e00415-18.

69. Luo LQ, Liao YJ, Jan LY, and Jan YN. Distinct Morphogenetic Functions of Similar Small Gtpases - Drosophila Drac1 Is Involved in Axonal Outgrowth and Myoblast Fusion. *Gene Dev.* 1994;8(15):1787-802.

70. Lee TM, and Luo LQ. Mosaic analysis with a repressible cell marker (MARCM) for neural development. *Trends Neurosci.* 2001;24(7):251-4.

71. Link N, Chung H, Jolly A, Withers M, Tepe B, Arenkiel BR, et al. Mutations in ANKLE2, a

ZIKA Virus Target, Disrupt an Asymmetric Cell Division Pathway in Drosophila Neuroblasts to Cause Microcephaly. *Developmental Cell.* 2019;51(6):713-29.

72. Link N, and Bellen HJ. Using to drive the diagnosis and understand the mechanisms of rare human diseases. *Development.* 2020;147(21):dev191411.

73. Bian S, Repic M, Guo Z, Kavirayani A, Burkard T, Bagley JA, et al. Author Correction: Genetically engineered cerebral organoids model brain tumor formation. *Nat Methods.* 2018;15(9):748.

74. Lancaster MA, Renner M, Martin CA, Wenzel D, Bicknell LS, Hurles ME, et al. Cerebral organoids model human brain development and microcephaly. *Nature.* 2013;501(7467):373-9.

Figures

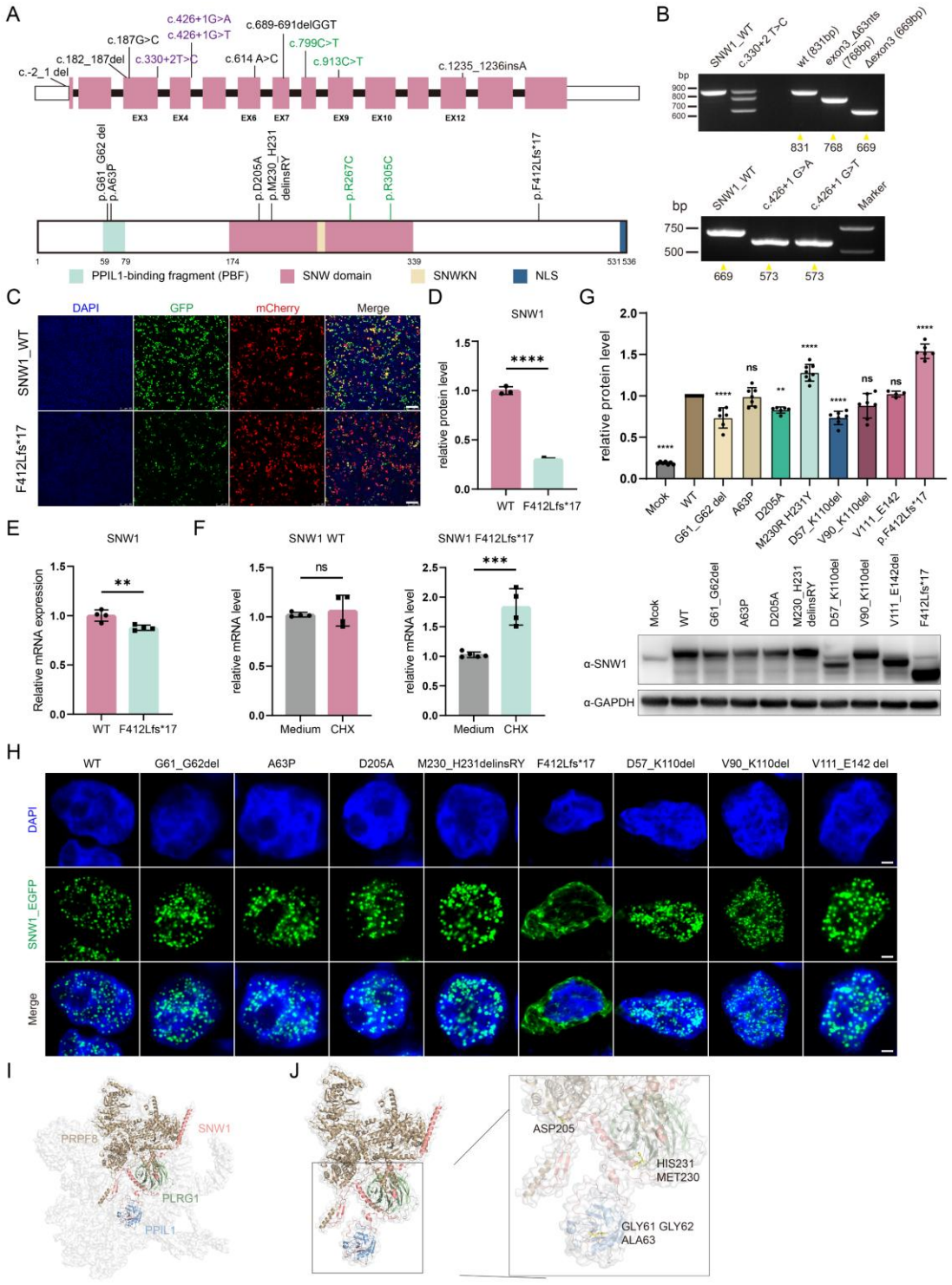

Figure 1. Mutations in *SNW1* lead to microcephaly and impair SNW1 functions in human.

(**A**) Schematic diagram of *SNW1* transcript (NM_012245.3, intron not to scale) (top panel) and schematic outline of the SNW1 protein domains (lower panel) with the locations of nine LOF variants identified in our study. The splice-donor variants are shown in purple. The two variants reported in the literature are shown in green. (**B**) The

c.330+2T>C construct showed complete skipping of exon 3 and partial 63 bp skip. The c.426+1G>A and c.426+1G>T constructs showed complete skipping of exon 4. (**C**) Fluorescence images of the HEK293T cells after transfection with SNW1_wildtype (WT) or F412Lfs*17 vectors. pmCherry-C1 was used as an internal control and co-transfected with the WT and F412Lfs*17 vectors at the same ratio. Scale bars = 100 μm. (**D**) Expression analysis of SNW1 by Western blotting was performed in lysates from HEK293T cells transfected with either SNW1 WT or F412Lfs*17 vectors. (**E**) qPCR analysis for SNW1 in HEK293T cells transfected with SNW1 WT or F412Lfs*17 vectors. (**F**) qPCR analysis for SNW1 in SNW1 wild-type (left) or F412Lfs*17 (right) HEK293T cells after stimulated by NMD inhibitor cycloheximide (100 μg/mL). (**G**) Overexpression of C-terminal FLAG-tagged WT and SNW1 variants in HEK293T cells. GAPDH serves as a loading control. Quantification of overexpressed Flag-tagged SNW1 proteins. (**H**) Effects of mutations on the localization of SNW1 in HEK293T cells. Fluorescence images were captured using laser scanning confocal microscopy (Leica TCS SP8) with 63 × oil glass. SNW1 (green) and DAPI (blue) are displayed. Scale bars = 2.5 μm. (**I, J**) Cryo-EM Structure of the human spliceosome ILS complex (PDB ID: 6id0) highlighting SNW1 (surface in pink) and its interacting proteins in the spliceosome, including PPIL1 (sky blue), PLRG1 (olive drab) and PRPF8 (brown). Residues in patients were observed to be located at the interface where SNW1 interacts with these proteins, suggesting changed in molecular interactions. Data are presented as mean ± SEM. $^{**}P < 0.01$, $^{***}P < 0.001$, $^{****}P < 0.0001$, ns, no significance.

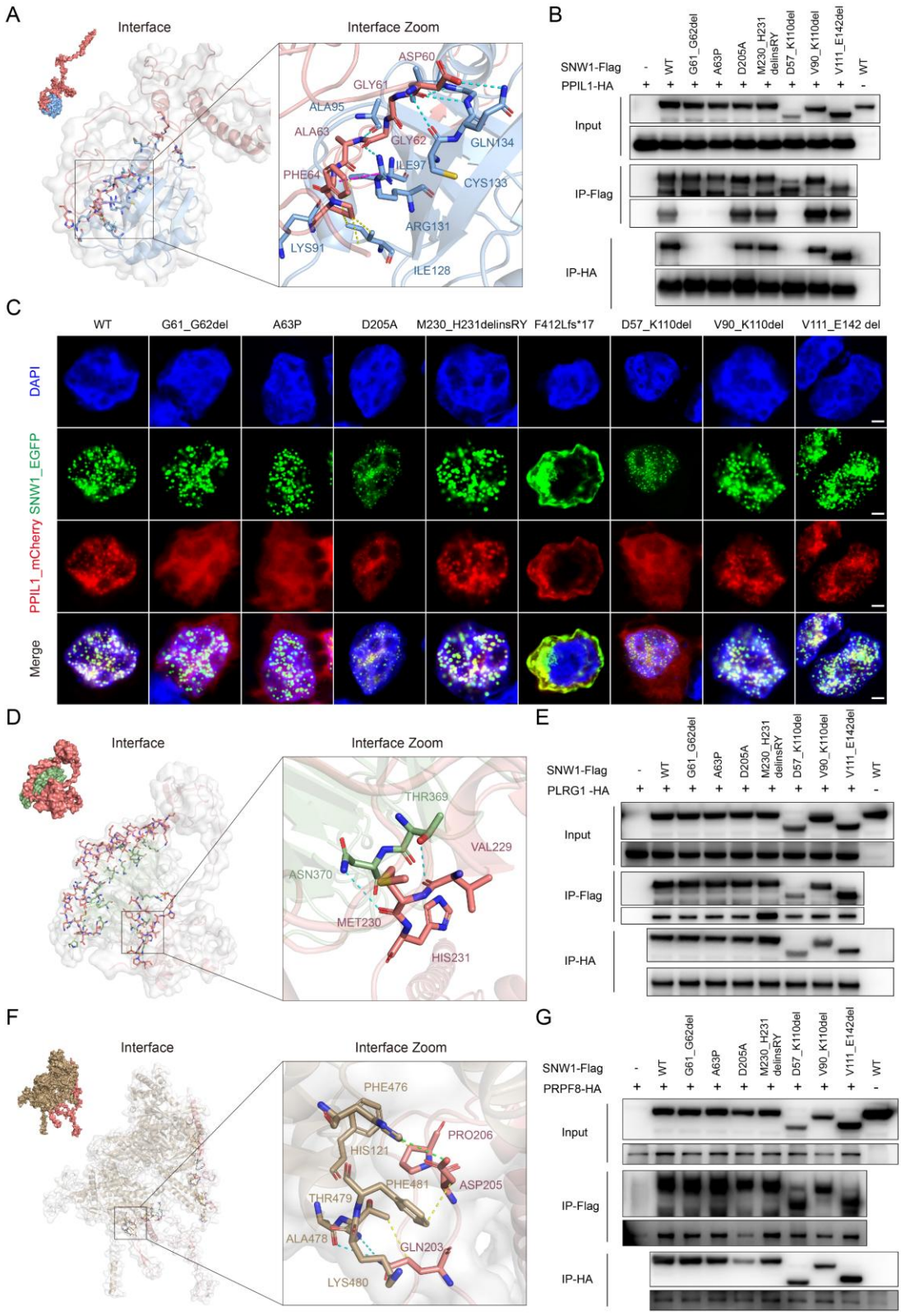

Figure 2. SNW1 interacted with PPIL1, PLRG1 and PRPF8.

(**A**) Structure-based protein interaction interface analysis between SNW1 (pink) and PPIL1 (sky blue), where interaction hotspot residues are labeled. (**B**) Coimmunoprecipitation (CoIP) of SNW1 and PPIL1 was performed. HEK293T cells were transfected with plasmids encoding SNW1-Flag and PPIL1-HA. The cell lysates

were subjected to anti-Flag and anti-HA immunoprecipitation (IP), followed by analysis via Western blotting. (**C**) Subcellular localization analysis of SNW1 and PPIL1. HEK293T cells were transfected with the plasmid encoding pEGFP-SNW1 and pmCherry-PPIL1 for 24 h, and then fixed and stained with DAPI. SNW1 (green), PPIL1 (red) and DAPI (blue) are displayed. Scale bars = 2.5 μm. (**D**) Structure-based protein interaction interface analysis between SNW1 (pink) and PLRG1 (olive drab), where interaction hotspot residues are labeled. (**E**) CoIP of SNW1 and PLRG1 was performed. HEK293T cells were transfected with plasmids encoding SNW1-Flag and PLRG1-HA. The cell lysates were subjected to anti-Flag and anti-HA IP, followed by analysis via Western blotting. (**F**) Structure-based protein interaction interface analysis between SNW1 (pink) and PRPF8 (brown), where interaction hotspot residues are labeled. (**G**) CoIP of SNW1 and PRPF8 was performed. HEK293T cells were transfected with plasmids encoding SNW1-Flag and PRPF8-HA. The cell lysates were subjected to anti-Flag and anti-HA IP, followed by analysis via Western blotting.

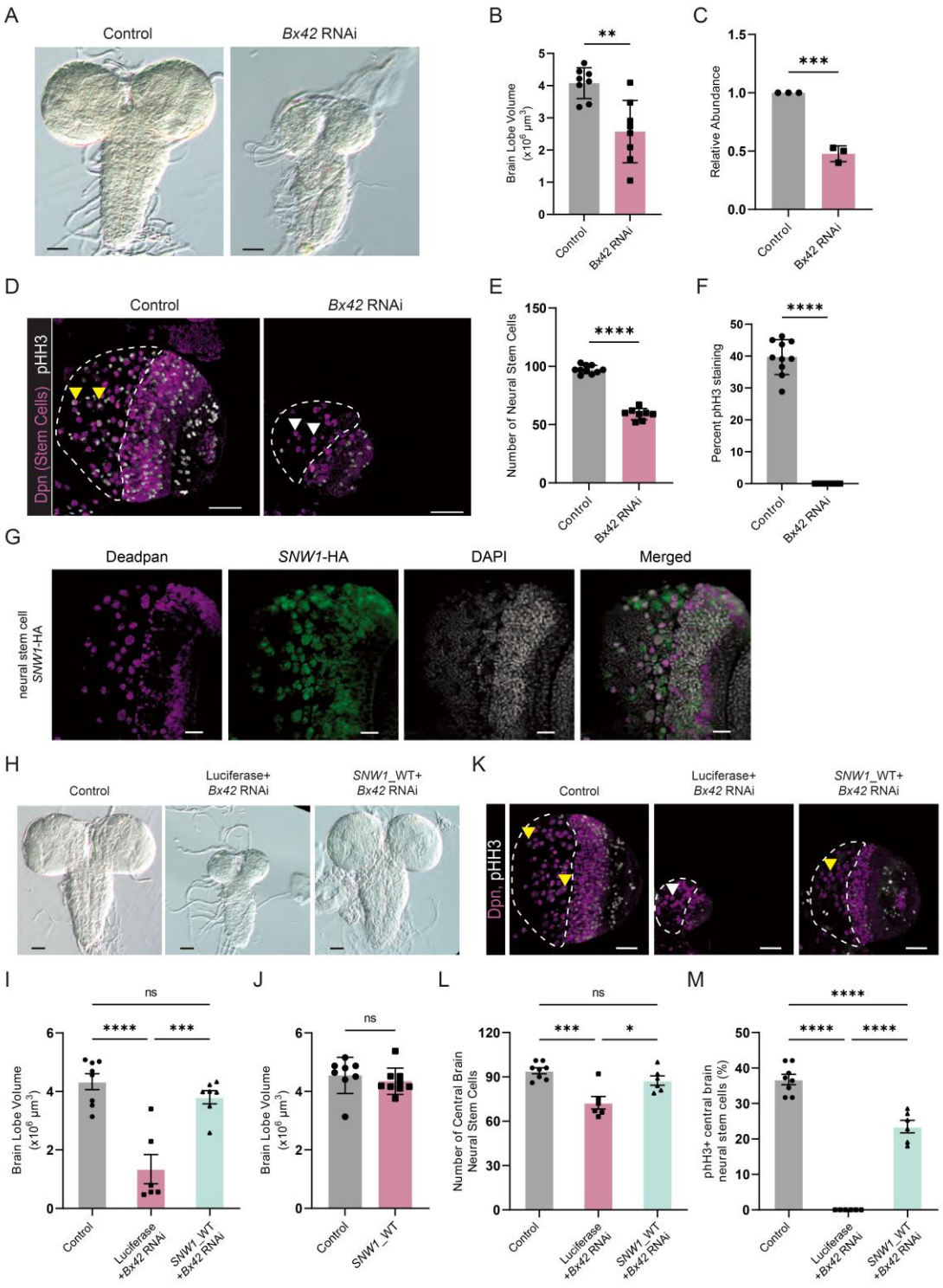

Figure 3. *Bx42* Knockdown in neural stem cells leads to reduced brain lobe volume, stem cell number, and percent proliferating stem cells.

(**A**) Images of third instar larval brains with knockdown of (A) *EGFP* (VALIUM22-EGFP.shRNA.1) or *Bx42* (TRiP.HMS00086) in neural stem cells (*inscuteable (insc)-GAL4*). (**B**) The brain lobe volume of *EGFP* (control) and *Bx42* knockdown in neural stem cells, each point representing one brain (n=10). Knockdown of *Bx42* in neural stem cells results in significantly reduced brain lobe volume compared to the control. (**C**) Normalized expression of *Bx42* transcript expression in control and *Bx42* RNAi

brains. *EGFP* or *Bx42* were knocked down in neurons, and third-instar brains were collected for qPCR. *Bx42* transcript expression was normalized to *RpL32* transcript expression. Knockdown of *Bx42* using the TRiP RNAi line has an efficiency of around 55%, where only 45% of the relative *Bx42* transcript is present in knockdown brains. (**D**) Confocal images of a single brain lobe from third instar larvae with knockdown of *EGFP* or *Bx42* in neural stem cells. Brains were stained for a nuclear marker of neural stem cells (Deadpan, Dpn) and phospho-Histone H3 (pHH3, marker for proliferating cells). The central brain region is outlined in white. (**E**) The number of Dpn+ neural stem cells in the central brain region in *EGFP* (n=10) and *Bx42* (n=8) neural stem cell knockdown *Drosophila*. Knockdown of *Bx42* in neural stem cells causes a significant reduction in the number of neural stem cells. (**F**) Proliferating cells were quantified by counting the percentage of Dpn+ cells with colocalized pHH3 puncta (yellow arrowheads) in the nucleus in *EGFP* (n=10) and *Bx42* (n=8) knockdown brains. Dpn+ cells without pHH3 puncta are noted with a white arrowhead. There is complete loss of proliferating neural stem cells in third instar larvae with *Bx42* knockdown using insc-*GAL4*. (**G**) SNW1-HA was expressed in neural stem cells (*insc-GAL4*) and stained with Dpn (magenta), HA (green), DAPI (white) to confirm presence of SNW1 protein in the nucleus of neural stem cells. (**H**) Images of third instar larval brains with knockdown of *EGFP*, *Luciferase* + *Bx42* RNAi, or *SNW1*_WT + *Bx42* RNAi in neural stem cells (*insc-GAL4*). (**I**) Brain lobe volume of genotypes from (H), each dot represents one brain. (**J**) The brain lobe volume of *Drosophila* expressing *SNW1* alone in neural stem cells was analyzed. No statistically significant difference was observed between the overexpression group and the control group, demonstrating that the heterologous expression of human *SNW1* in *Drosophila* neural stem cells does not induce nonspecific developmental abnormalities. (**K**) Confocal images of a single brain lobe from third instar larvae with knockdown of *EGFP, Luciferase* + *Bx42* RNAi, or *SNW1*_WT + *Bx42* RNAi in neural stem cells. The central brain region is outlined in white. (**L**) Proliferating cells were quantified in *EGFP* (n=8), *Luciferase* + *Bx42* RNAi (n=6), and *SNW1*_WT + *Bx42* RNAi (n=6) knockdown brains. (**M**) Proliferating cells were quantified by counting the percentage of Dpn+ cells with colocalized pHH3 puncta (yellow arrowheads) in the nucleus in *EGFP* (n=8), *Luciferase* + *Bx42* RNAi (n=6), and *SNW1*_WT + *Bx42* RNAi (n=6) knockdown brains. Data are presented as mean ± SEM. *$P < 0.05$, **$P < 0.01$, ***$P < 0.001$, ****$P < 0.0001$, ns, no significance.

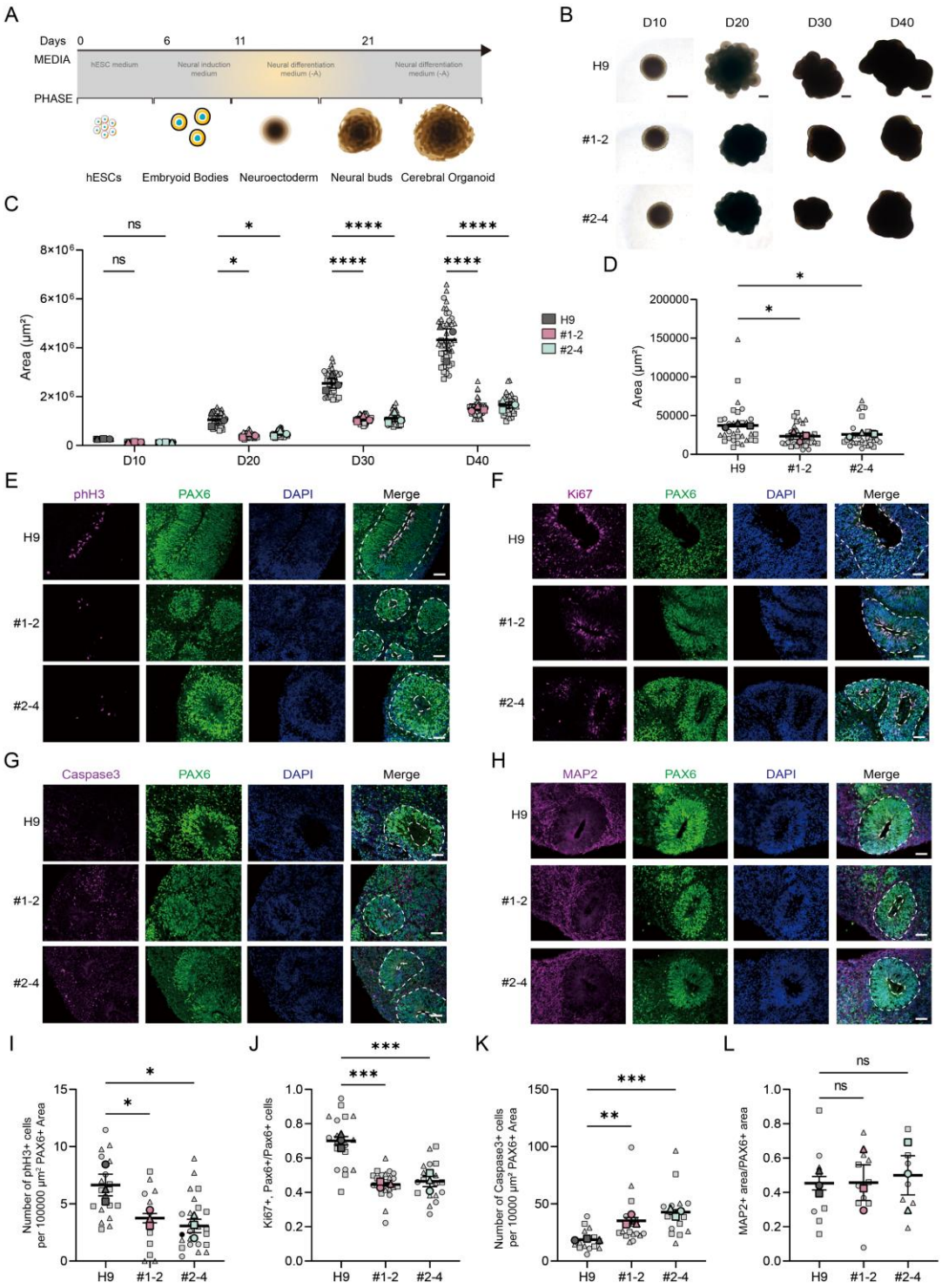

Figure 4. Developmental progression and phenotypic analysis of *SNW1*$^{+/-}$ cerebral organoids reveals altered size and neural stem cells properties.

(**A**) Schematic of making cerebral organoid based on Lancaster methods. (**B**) Representation images of H9 and SNW1$^{+/-}$ brain organoids cultured for 10, 20, 30, and 40 days. Scale bar: 500 µm. (**C**) The size of brain organoids from different groups was quantified at multiple time points across three independent experiments. (**D**) The VZ-like PAX6+ rosette area was quantified, with each data point representing an individual rosette. Data were collected from three independent experiments. (**E-H**)

Immunofluorescent staining was performed on sections of wild-type and *SNW1*$^{+/-}$ brain organoids cultured for 45 days. PAX6 was used to label the VZ-like rosette area, which was further stained with pHH3 (**E**), Ki67 (**F**), Caspase3 (**G**), and MAP2 (**H**). Scale bars = 50 μm. (**I**) Quantification of the ratio of pHH3+ cells per 100000 μm^2 PAX6+ area of each rosette. Each plot represented an individual rosette. (**J**) Quantification of the ratio of Ki67 and PAX6 double-positive cells versus the total number of PAX6+ cells of each rosette. Each plot represented an individual rosette. (**K**) Quantification of the ratio of Caspase3+ cells per 100000 μm^2 PAX6+ area of each rosette. Each plot represented an individual rosette. (**L**) Quantification of the ratio of MAP2 and PAX6 double-positive cells versus the total number of PAX6+ cells of each rosette. Each plot represented an individual rosette. The proliferating rosettes and apical surface adjust to ventricle-like regions were highlight by white dash lines. VZ-like rosette area was indicated by white dash lines. Small gray symbols represent size measurements of single hCOs (technical replicates); Different symbol shapes denote three independent biological replicate experiments (n = 3 per group), large colored symbols indicate means of technical replicates within each biological replicate. Data are presented as mean ± SEM. Statistical significance was tested by one-way ANOVA. *$P < 0.05$, **$P < 0.01$, ***$P < 0.001$, ****$P < 0.0001$, ns, no significance.

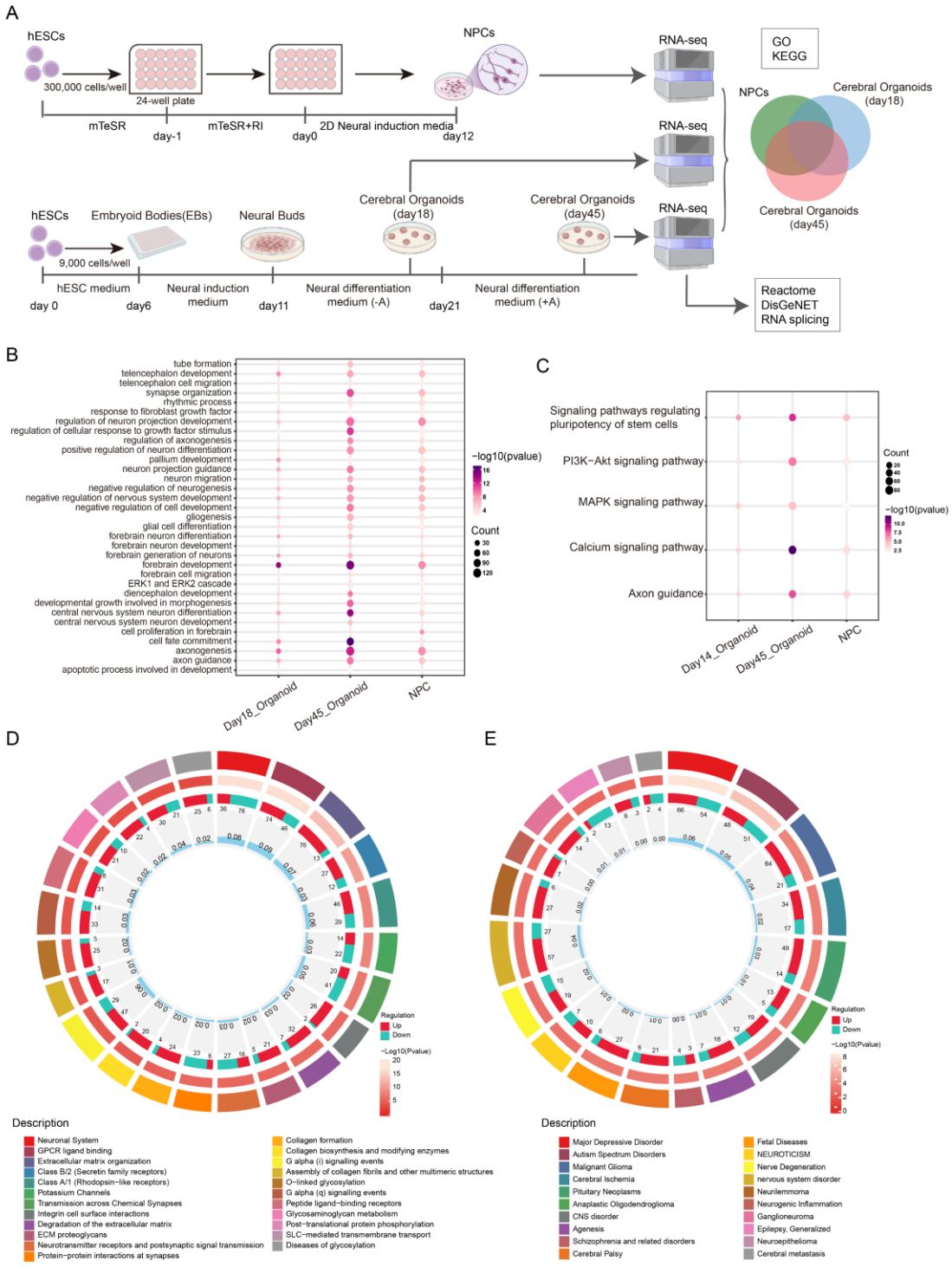

Figure 5. Developmental and transcriptomic analysis of human cerebral organoids derived from *SNW1*$^{+/-}$ hESCs.

(**A**) Schematic overview of the experimental design. human embryonic stem cells (hESCs) were differentiated into neural progenitor cells (NPCs) over 12 days and into cerebral organoids over 45 days. NPCs cultured for 18 days, cerebral organoids cultured for 18 days, and cerebral organoids cultured for 45 days were collected for bulk RNA-seq analysis. (**B**) Gene Ontology (GO) biological process analysis of differentially expressed genes is shown, highlighting common enriched terms across the three groups

(NPCs, Day 18 organoids, and Day 45 organoids). (**C**) KEGG pathway enrichment analysis of differentially expressed genes is presented, displaying shared enriched pathways among the three groups (NPCs, Day 18 organoids, and Day 45 organoids). (**D**) Reactome pathway enrichment circos plot for 45-day cerebral organoids. For each Reactome term around the circle (outermost ring), the adjacent ring showed up-regulated (red) versus down-regulated (teal) gene counts; the next inner ring showed -log10(pvalue) as a heat map; the innermost ring displays gene ratio bars. (**E**) DisGeNET disease association circos plot for 45-day cerebral organoids, plotted in the same concentric-ring format as in (D).

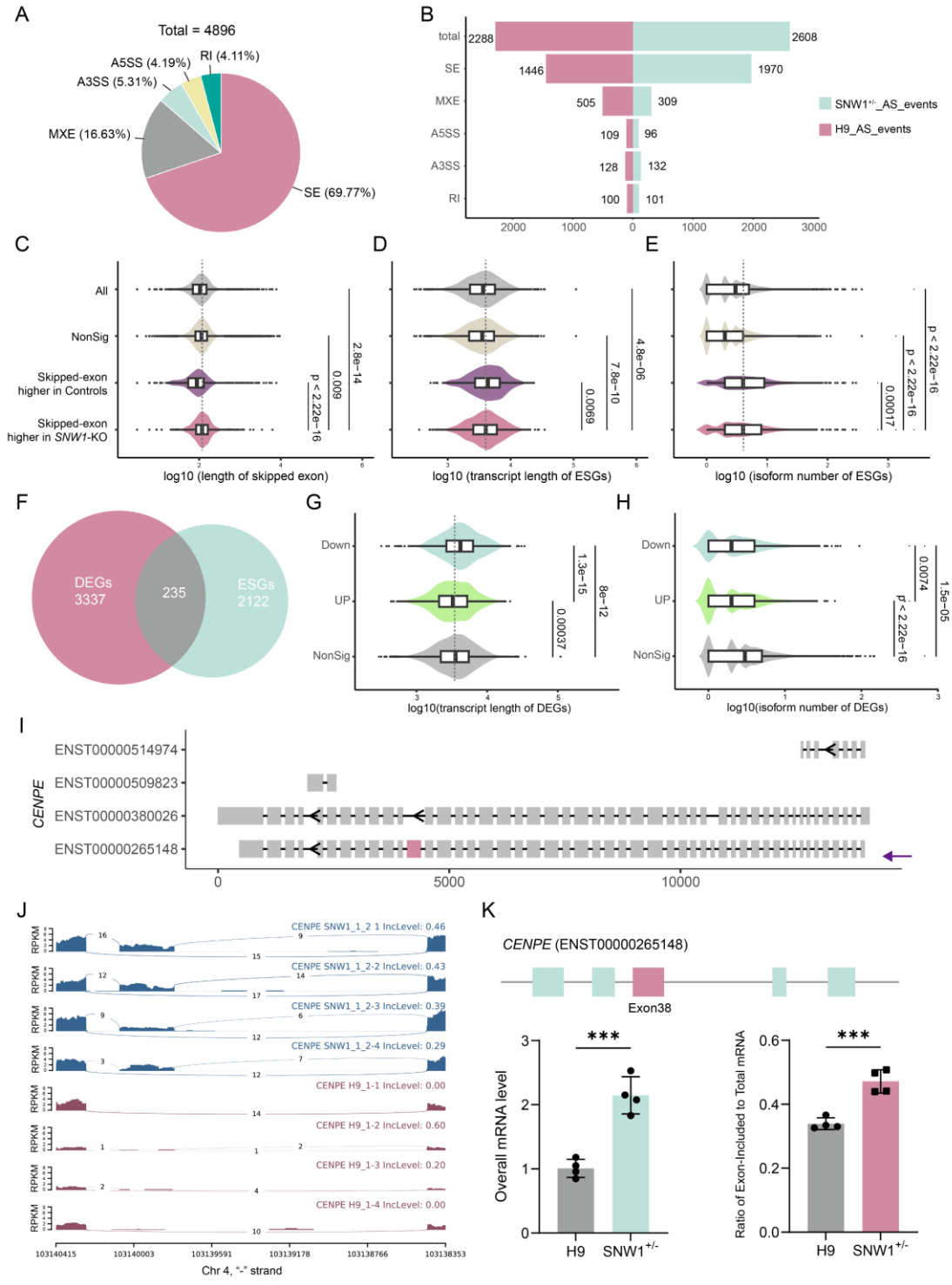

Figure 6. Splicing integrity defects in *SNW1*$^{+/-}$ hCOs.

(**A**) Impact of SNW1 depletion on five major types of AS events detected with rMATS in hCOs (45-day-old). SE were most affected, followed by MXE, A3SS, A5SS, RI. (**B**) Columns showing numbers of significant events with higher inclusion level in *SNW1*$^{+/-}$ (sky blues) or controls (pink). (**C**) Distribution of differential splicing identified by rMATS in *SNW1*$^{+/-}$ or control, on the basis of skipped-exon length. Exons with long length show significantly skipped higher in *SNW1*$^{+/-}$ hCOs. *P* value from Wilcoxon test. (**D**) Violin plot of transcript length significant exon skipping genes (ESGs). *P* value

from Wilcoxon test. (**E**) Violin plot of isoform numbers of ESGs. *P* value from Wilcoxon test. (**F**) Venn diagram of overlap of DEGs and ESGs. (**G** and **H**) Violin plot of transcript length of DEGs compared to non-significant genes. NonSig, non-significant genes (grey); UP, upregulated (light-green); Down, downregulated (sky blue). *P* value from Wilcoxon test. (**I**) Schematic representation of human *CENPE* transcripts isoforms. The purple arrows indicate the MANE-selected canonical transcripts. The identified exons in the rMATS analysis are marked in pink. (**J**) Sashimi plots of read density of *CENPE* transcript in 4 $SNW1^{+/-}$ (#1-2) and 4 control brain organoids revealed that $SNW1^{+/-}$ hCOs exhibited retention of exon 38, while wild-type tended to skip this exon. (**K**) RT-PCR validations of SE events of *CENPE* in wildtype and $SNW1^{+/-}$ brain organoids (#1-2). Top: Schematic diagrams of *CENPE* transcript. The pink boxes represent the skipped exons. Bottom: validation of significant exon skipping events by semiquantitative RT-PCR using *GAPDH* as reference gene. Relative level of overall mRNA (sky blue); ratio of Exon-included mRNA to total mRNA (pink). ***$P < 0.001$.

Table

Table 1. Clinical Information of Selected Patients.

	Individual 1[A]	Individual 2[B]	Individual 3[C]	Individual 4[D]	Individual 5[E]	Individual 6[F]	Individual 7[G]	Individual 8[H]	Individual 9[I]
Mutation cDNA	c.182_187del	c.691_689delinsGGT	c.330+2T>C	c.614A>C	c.-2_1del	c.187G>C	c.1235_1236insA	c.426+1G>A	c.426+1G>T
Mutation protein	p.Gly61_Gly62del	p.M230_H231delinsRY	?	p.Asp205Ala	p.Met1?	p.Ala63Pro	p.Phe412Leufs*17	p.Lys111_Glu142 del	p.Lys111_Glu142 del
Gender	F	F	F	M	F	M	M	NA	NA
Head circumference (HC) at birth (cm)	28 (-4.6 SD)	29 (-3.93 SD)	32 (-1.9 SD)	33 (-1.27 SD)	NA	NA	NA	30 (-2.85 SD)	NA
Age at last evaluation	20	8 y	18 y 7m	7 y	24 y	3 y 9 m	19w5d gestational age	9 y 4m	9 y
HC at last evaluation (cm)	45 (-8.8 SD)	39 (-10.3 SD)	47 (-6.9 SD)	48 (-3.5 SD)	49.3 (-4.52 SD)	44.5 (-3.6 SD)	NA	44 (-6.5 SD)	39.4 (-6.93 SD)
height at last evaluation (cm)	150 (-2.04 SD)	105 (-4.0 SD)	152 (-1.7SD)	116 (-1.5 SD)	157 (-1.19 SD)	101	NA	130 (-0.23 SD)	122.2 (-3.41 SD)
Weight at last evaluation (kg)	27 (-4.55 SD)	15 (-3.2 SD)	40 (-2.6 SD)	20 (-1.5 SD)	54.1 (-0.42 SD)	13 (-1.74 SD)	NA	20 (-2.1 SD)	24.9 (-2.41 SD)
Seizures	Yes	Yes	Yes	Yes	No	Yes	NA	Y	Y
Estimated degree of ID	Severe	Severe	Profound	Moderate	Moderate	Moderate	NA	Severe	Severe
Autistic features	No	Yes	No	Yes	No	Yes	NA	N	NA
Brain malformation	Yes	NA	Yes	NA	Yes	NA	Yes	Y	Y
Facial Dysmorphism	Yes	Yes	Yes	Yes	Yes	No	Yes	NA	Y

Note: The source units for the individuals listed in this table are provided in the supplementary materials.